with Nujol. The X-ray data were collected at 200 K on a Rigaku Raxis-RAPID Imaging Plate diffractometer with graphite monochromated Mo Kα ($\lambda = 0.71075$ Å). The basic crystallographic parameters are listed in Table S1 (See Supporting Information). A symmetry-related absorption correction using the program ABSCOR[33] was applied, which resulted in transmission factors ranging from 0.43 to 0.49 for **BCNCPB–OH** and 0.42 to 0.53 for **BCNCPB–O–NEt$_4$**. The structure was solved by the direct method (SHELXS-97[34] for **BCNCPB–OH** and SIR92[35] for **BCNCPB–O–NEt$_4$**) and expanded using Fourier techniques using *teXsan* crystallographic software[36] and SHELXL-97.[37] Non-hydrogen atoms were refined anisotropically. The positions of OH and NH were refined using fixed thermal parameters, and the other hydrogen atoms were placed at calculated positions.

Crystal Data. **BCNCPB–OH:** $C_{13}H_8BrCl_2NO_2$, $M = 361.02$, orthorhombic, $a = 23.15(2)$, $b = 15.73(2)$, $c = 7.126(7)$ Å, $U = 2594(10)$ Å^3, $T = 200$ K, space group *Pccn* (no. 56), $Z = 8$, $\mu = 35.84$ cm^{-1}, 22578 reflections measured, 2836 unique ($R_{int} = 0.096$), $R_1 = 0.036$ ($I > 2\sigma$), $wR_2 = 0.070$ (all data).

BCNCPB–O–NEt$_4$: $C_{21}H_{27}BrCl_2N_2O_2$, $M = 490.27$, orthorhombic, $a = 7.307(4)$, $b = 16.18(1)$, $c = 18.99(1)$ Å, $U = 2245(8)$ Å^3, $T = 200$ K, space group $P2_12_12_1$ (no. 19), $Z = 4$, $\mu = 20.93$ cm^{-1}, 21267 reflections measured, 2935 unique ($R_{int} = 0.045$), $R_1 = 0.028$ ($I > 2\sigma$), $wR_2 = 0.048$ (all data).

One of the authors (DK) expresses his special thanks to the center of excellence (21COE) program "Creation of Integrated EcoChemistry of Osaka University".

References

1 A. A. Lugovskoy, A. I. Degterev, A. F. Fahmy, P. Zhou, J. D. Gross, J. Yuan, and G. Wagner, *J. Am. Chem. Soc.*, **124**, 1234 (2002).

2 A. Degterev, A. Lugovskoy, M. Cardone, B. Mulley, G. Wagner, T. Mitchison, and J. Yuan, *Nat. Cell Biol.*, **3**, 173 (2001).

3 X. Gao, X. Wen, L. Esser, B. Quinn, L. Yu, C.-A. Yu, and D. Xia, *Biochemistry*, **42**, 9067 (2003).

4 H. Miyoshi, N. Tokutake, Y. Imaeda, T. Akagi, and H. Iwamura, *Biochim. Biophys. Acta*, **1229**, 149 (1995).

5 N. Tokutake, H. Miyoshi, T. Satoh, T. Hatano, and H. Iwamura, *Biochim. Biophys. Acta*, **1185**, 271 (1994).

6 D. L. Selwood, D. J. Livingstone, J. C. W. Comley, A. B. O'Dowd, A. T. Hudson, P. Jackson, K. S. Jandu, V. S. Rose, and J. N. Stables, *J. Med. Chem.*, **33**, 136 (1990).

7 Z. Wawrzak, T. Sandalova, J. J. Steffens, G. S. Basarab, T. Lundqvist, Y. Lindqvist, and D. B. Jordan, *Proteins: Struct., Funct., Genet.*, **35**, 425 (1999).

8 C. N. Hodge and J. Pierce, *Bioorg. Med. Chem. Lett.*, **3**, 1605 (1993).

9 R. L. Williamson and R. L. Metcalf, *Science*, **158**, 1694 (1967).

10 B. T. Storey, D. F. Wilson, A. Bracey, S. L. Rosen, and S. Stephenson, *FEBS Lett.*, **49**, 338 (1975).

11 H. Terada, S. Goto, K. Yamamoto, I. Takeuchi, Y. Hamada, and K. Miyake, *Biochim. Biophys. Acta*, **936**, 504 (1988).

12 M. J. Macielag, J. P. Demers, S. A. Fraga-Spano, D. J. Hlasta, S. G. Johnson, R. M. Kanojia, R. K. Russell, Z. Sui, M. A. Weidner-Wells, H. Werblood, B. D. Foleno, R. M. Goldschmidt, M. J. Loeloff, G. C. Webb, and J. F. Barrett, *J. Med. Chem.*, **41**, 2939 (1998).

13 D. J. Hlasta, J. P. Demers, B. D. Foleno, S. A. Fraga-Spano, J. Guan, J. J. Hilliard, M. J. Macielag, K. A. Ohemeng, C. M. Sheppard, Z. Sui, G. C. Webb, M. A. Weidner-Wells, H. Werblood, and J. F. Barrett, *Bioorg. Med. Chem. Lett.*, **8**, 1923 (1998).

14 H. Kim, L. Esser, M. B. Hossain, D. Xia, C.-A. Yu, J. Rizo, D. van der Helm, and J. Deisenhofer, *J. Am. Chem. Soc.*, **121**, 4902 (1999).

15 K. M. Kim, C. D. Giedt, G. Basañez, J. W. O'Neil, J. J. Hill, Y.-H. Han, S.-P. Tzung, J. Zimmerberg, D. M. Hockenbery, and K. Y. J. Zhang, *Biochemistry*, **40**, 4911 (2001).

16 S.-P. Tzung, K. M. Kim, G. Basañez, C. D. Giedt, J. Simon, J. Zimmerberg, K. Y. J. Zhang, and D. M. Hockenbery, *Nat. Cell Biol.*, **3**, 183 (2001).

17 F. Mu, E. Hamel, D. J. Lee, D. E. Pryor, and M. Cushman, *J. Med. Chem.*, **46**, 1670 (2003).

18 H. Suezawa, M. Hirota, T. Yuzuki, Y. Hamada, I. Takeuchi, and M. Sugiura, *Bull. Chem. Soc. Jpn.*, **73**, 2335 (2000).

19 W. L. Mock and D. C. Y. Chua, *J. Chem. Soc., Perkin Trans. 2*, **1995**, 2069.

20 D. Welti, *Spectrochim. Acta*, **22**, 281 (1966).

21 M. Sattler, H. Liang, D. Nettesheim, R. P. Meadows, J. E. Harlan, M. Eberstadt, H. S. Yoon, S. B. Shuker, B. S. Chang, A. J. Minn, C. B. Thompson, and S. W. Fesik, *Science*, **275**, 983 (1997).

22 A. Fahmy and G. Wagner, *J. Am. Chem. Soc.*, **124**, 1241 (2002).

23 N. Ueyama, M. Inohara, A. Onoda, T. Ueno, T. Okamura, and A. Nakamura, *Inorg. Chem.*, **38**, 4028 (1999).

24 A. Onoda, Y. Yamada, J. Takeda, Y. Nakayama, T. Okamura, M. Doi, H. Yamamoto, and N. Ueyama, *Bull. Chem. Soc. Jpn.*, **77**, 321 (2004).

25 C. Hansch, A. Leo, and R. W. Taft, *Chem. Rev.*, **91**, 165 (1991).

26 Y. Mido and T. Okuno, *J. Mol. Struct.*, **82**, 29 (1982).

27 Y. Mido, M. Sakoda, and K. Fujiwara, *J. Mol. Struct.*, **350**, 205 (1995).

28 A. Onoda, T. Okamura, H. Yamamoto, and N. Ueyama, *Acta Crystallogr.*, **E59**, o1202 (2003).

29 H. Endo, M. Hirota, Y. Ito, I. Takeuchi, and Y. Hamada, *Bull. Chem. Soc. Jpn.*, **55**, 1564 (1982).

30 A. Onoda, Y. Yamada, T. Okamura, M. Doi, H. Yamamoto, and N. Ueyama, *J. Am. Chem. Soc.*, **124**, 1052 (2002).

31 A. I. Biggs and R. A. Robinson, *J. Chem. Soc.*, **1961**, 388.

32 M. A. Weidner-Wells and S. A. Fraga-Spano, *Synth. Commun.*, **26**, 2775 (1996).

33 T. Higashi, "Program for Absorption Correction," Rigaku Corporation, Tokyo, Japan (1995).

34 SHELXS-97: G. M. Sheldrick, "Program for the Refinement of Crystal," University of Göttingen, Germany (1997).

35 A. Altomare, M. C. Burla, M. Camalli, M. Cascarano, C. Giacovazzo, A. Guagliardi, and G. Polidori, *J. Appl. Crystallogr.*, **27**, 435 (1994).

36 teXsan: "Crystal Structure Analysis Package," Molecular Structure Corporation (1985, 1999).

37 SHELXL-97: G. M. Sheldrick, "Program for the Refinement of Crystal," University of Göttingen, Germany (1997).

Accelerated Publication

THE JOURNAL OF BIOLOGICAL CHEMISTRY
Vol. 280, No. 2, Issue of January 14, pp. 857–860, 2005

Nuclear Translocation of Caspase-3 Is Dependent on Its Proteolytic Activation and Recognition of a Substrate-like Protein(s)*[S]

Received for publication, November 19, 2004
Published, JBC Papers in Press, November 29, 2004,
DOI 10.1074/jbc.C400538200

Shinji Kamada‡§¶‖, Ushio Kikkawa§, Yoshihide Tsujimoto¶, and Tony Hunter‡**

From the ‡Molecular and Cell Biology Laboratory, The Salk Institute, La Jolla, California 92037, the §Biosignal Research Center, Kobe University, 1-1 Rokkodai-cho, Nada-ku, Kobe, Hyogo 657-8501, Japan, and the ¶Laboratory of Molecular Genetics, Department of Post-Genomics and Diseases, Osaka University Medical School and Graduate School of Medicine, 2-2 Yamadaoka, Suita, Osaka 565-0871, Japan

Caspase-3 is thought to play an important role(s) in the nuclear morphological changes that occur in apoptotic cells and many nuclear substrates for caspase-3 have been identified despite the cytoplasmic localization of procaspase-3. Therefore, whether activated caspase-3 is localized in the nuclei and how active caspase-3 has access to its nuclear targets are important and unresolved questions. Here we confirmed nuclear localizations for both caspase-3-p17 and caspase-3-p12 subunits of active caspase in apoptotic cells using subcellular fractionation analysis. We also prepared polyclonal and monoclonal antibodies specific for active caspase-3 to define the subcellular localization of active caspase-3. Immunocytochemical observations using anti-active caspase-3 antibodies showed nuclear accumulation of active caspase-3 during apoptosis. In addition, caspase-3, but not caspase-7, translocated from the cytoplasm into the nucleus after induction of apoptosis. Mutations at the cleavage site between the p17 and p12 subunits and the substrate recognition site for the P3 amino acid of the DXXD substrate cleavage motif inhibited nuclear translocation of caspase-3, indicating that nuclear transport of active caspase-3 required proteolytic activation and substrate recognition. These results suggest that active caspase-3 is translocated in association with a substrate-like protein(s) from the cytoplasm into the nucleus during progression through apoptosis.

Apoptosis is a fundamental cellular process involved in many biological phenomena, including morphogenesis and maintenance of tissue homeostasis. Apoptosis is morphologically characterized by a dramatic execution phase that includes loss of cell volume, plasma membrane blebbing, and chromatin condensation followed by packaging of the cellular contents into membrane-enclosed vesicles called apoptotic bodies. These changes reflect complex biochemical events carried out by a family of cysteine proteases called caspases (1). Caspases are divided into initiator caspases with long prodomains (caspase-8, -9, and -10) and effector caspases with short prodomains (caspase-3, -6, and -7). Initiator caspases activate effector caspases, which in turn cleave intracellular substrates, resulting in the dramatic morphological and biochemical changes characteristic of apoptosis (2–4).

Caspase-3 has been implicated as a key mediator of apoptosis in mammalian cells and is synthesized as a latent proenzyme composed of 277 amino acids (5–9). In response to various death signals, the caspase-3 proenzyme is cleaved by initiator caspases at Asp^{28} and Asp^{175} to generate the active large (p17) and small (p12) subunits, forming an active heterotetramer. Although the precursor form of caspase-3 is localized in the cytoplasm, caspase-3 plays essential roles in the nuclear changes in apoptotic cells (9, 10). These results suggested that some cytoplasmic substrates translocate into the nucleus after cleavage by caspase-3 leading to nuclear morphological changes. In this scenario, caspase-activated DNase (CAD)[1]/DNA fragmentation factor (DFF) 40 and apoptotic chromatin condensation inducer in the nucleus (Acinus) were identified in the cytoplasmic fraction of apoptotic cells (11–13). However, CAD/DFF40 and Acinus were suggested to be localized in the nucleus even before apoptosis induction (12–14). Furthermore, many substrates for caspase-3 have been identified in the nucleus (2–4, 15). Therefore, caspase-3 seems to translocate from the cytoplasm into the nucleus after apoptosis induction, and it was proposed that active caspase-3 is translocated into nuclei by simple diffusion after disruption of nuclear-cytoplasmic barrier (16). However, the precise molecular mechanism of nuclear translocation of active caspase-3 is still unknown.

In the present study, we have demonstrated the nuclear localization of active caspase-3 in apoptotic cells by using antibodies specific for the large and small subunits of active caspase-3. Furthermore, we have shown that the nuclear translocation of active caspase-3 required proteolytic activation and substrate recognition by using caspase-3 mutants, suggesting that the nuclear translocation of active caspase-3 is not mediated by simple diffusion but is operated by an active transport system.

EXPERIMENTAL PROCEDURES

Cell Culture and Apoptosis Induction—HepG2 cells were cultured in RPMI 1640 medium with 10% fetal bovine serum (FBS). For induction of apoptosis, HepG2 cells were treated with 1 μg/ml of an agonistic anti-Fas antibody (CH-11; Kamiya Biomedical Co.) in the presence of 0.2 μg/ml actinomycin D or with 200 μg/ml etoposide. Transfection was performed using GenePORTER 2 (Gene Therapy Systems) according to the manufacturer's instructions.

* This work was supported in part by grants-in-aid for Scientific Research on Priority Areas from the Ministry of Education, Science, Sports, and Culture of Japan (to S. K.) and by Public Health Service Grants CA82863 and CA14195 from the NCI (to T. H.). The costs of publication of this article were defrayed in part by the payment of page charges. This article must therefore be hereby marked "*advertisement*" in accordance with 18 U.S.C. Section 1734 solely to indicate this fact.

[S] The on-line version of this article (available at http://www.jbc.org) contains supplemental Experimental Procedures, Results, and Fig. S1.

‖ To whom correspondence may be addressed. Tel.: 81-78-803-5965; Fax: 81-78-803-5972; E-mail: skamada@kobe-u.ac.jp.

** Frank and Else Schilling American Cancer Society Professor. To whom correspondence may be addressed: Molecular and Cell Biology Laboratory, The Salk Inst., 10010 North Torrey Pines Rd., La Jolla, CA 92037. Tel.: 858-453-4100; Fax: 858-457-4765; E-mail: hunter@salk.edu.

[1] The abbreviations used are: CAD, caspase-activated DNase; DFF, DNA fragmentation factor; GFP, green fluorescent protein; TXRD, Texas Red; PBS, phosphate-buffered saline; pAb, polyclonal antibody; PKC, protein kinase C; NPC, nuclear pore complex.

Subcellular Fractionation—For preparation of digitonin-lysed cell fractions, cells were washed with PBS and suspended in PBS followed by lysis with 0.3 mg/ml digitonin for 3 min at 37 °C and centrifuged at 12,000 × *g* for 5 min at 4 °C. The pellet and supernatant fractions were used for immunoblot analysis with the pellet fraction including nuclei and heavy membranes and the supernatant fraction containing cytoplasm and light membranes.

For preparation of subcellular fractions, cells were washed with PBS and suspended in hypotonic solution (10 mM Hepes (pH 7.4), 10 mM $MgCl_2$, 42 mM KCl, 10 μM lactacystin) for 5 min on ice. Cells were lysed using a Dounce homogenizer and centrifuged at 600 × *g* for 10 min to collect crude nuclei that were further purified as described below. The supernatant was further centrifuged at 100,000 × *g* for 90 min. The pellet and supernatant were used as membrane and cytoplasmic fractions, respectively. The crude nuclear fraction was passed through a 27-gauge needle several times, extensively washed with hypotonic solution, and centrifuged through a 2 M sucrose cushion at 150,000 × *g* for 60 min. The pellet was used as a purified nuclear fraction. Nonidet P-40-treated nuclei were prepared by washing the purified nuclei with hypotonic solution containing 0.5% Nonidet P-40 to remove contaminating membranes.

Antibodies—Anti-active caspase-3 polyclonal (2622) and monoclonal (CS-1) antibodies, which recognize caspase-3-p12, were generated (see supplemental material). Anti-caspase-3 monoclonal antibody (C31720) was obtained from Transduction Laboratories; anti-caspase-3 polyclonal antibodies (sc-1224), anti-PKC δ polyclonal antibodies (sc-937), and anti-lamin B1 polyclonal antibodies (sc-6217) were from Santa Cruz Biotechnology; anti-active caspase-3 pAb (G7481) was from Promega; anti-green fluorescent protein (GFP) monoclonal antibody (8371) from Clontech; and anti-caspase-3 polyclonal antibodies (9662) was from Cell Signaling Technology.

Fluorescence Microscopy—For immunofluorescence analysis, cells were fixed with 3.7% formaldehyde in PBS for 10 min, washed with PBS twice, permeabilized in 0.5% Triton X-100 in PBS for 10 min, and washed with PBS twice. Cells were then incubated with primary antibodies in PBS containing 1% BSA overnight at 4 °C. After washing with PBS twice, cells were incubated with Texas red (TXRD)-, fluorescein isothiocyanate-, Alexa Fluor 488-, or Cy3-labeled secondary antibodies for 10 min at room temperature and washed with PBS twice. After staining nuclei with 10 μM Hoechst 33342 (Calbiochem), cells were examined under a fluorescence microscope (Leitz Laborlux) or a confocal laser scanning microscope (Carl Zeiss).

Plasmid Constructions—The wild type procaspase-3 cDNA fragment was cloned into the EcoRI site of pUC-CAGGS (17) to generate pCAG-casp3. To construct expression plasmids for caspase fused to the N terminus of GFP, PCR was carried out using caspase-3 and caspase-7 cDNAs as templates. The fragments encoding caspase-3 or caspase-7 were cloned into the EcoRI-BamHI site of pEGFP-N1 (Clontech) to generate pcasp3-Wt-GFP or pcasp7-Wt-GFP. To generate C163S, D175A, R64E, and R207E mutations, a PCR method employing mutagenic oligonucleotide primers was used. Caspase-3 cDNAs containing these mutations were cloned into the EcoRI-BamHI site of pEGFP-N1 to generate pcasp3-C163S-GFP, pcasp3-D175A-GFP, pcasp3-R64E-GFP, and pcasp3-R207E-GFP.

RESULTS AND DISCUSSION

Although it has been widely accepted that procaspase-3 is cleaved to generate the active form in the cytoplasm, the enzymatic activity of capase-3-like proteases can be found in the nuclear fraction of apoptotic cells (18–20). It is, however, necessary to determine whether activated caspase-3 itself is present in the nuclei of apoptotic cells, as opposed to other caspases such as caspase-7 and -8 that can also cleave caspase-3 substrates (21, 22). The p17 subunit of active caspase-3 is detected not only in the cytoplasmic and mitochondrial fractions but also in the nuclear fraction of apoptotic cells (23). However, the localization of the p12 subunit of active caspase-3 remained to be determined, which is important, because caspase-3 enzymatic activity requires both p17 and p12 subunits. Therefore, we initially investigated the localization of the caspase-3-p12 subunit. HepG2 cells treated with or without an agonistic anti-Fas antibody were separated into pellet and supernatant fractions after lysis with digitonin, followed by immunoblotting (Fig. 1*A*). Although procaspase-3 was present in the supernatant fraction irrespective of induction of apoptosis, the caspase-3-p12 subunit was present in both the pellet fraction (including nuclei) and the supernatant fraction after induction of apoptosis. Subcellular fractionation was used to confirm the nuclear localization of active caspase-3 in apoptotic cells. Since active caspase-3 may be degraded by the ubiquitin-proteasome pathway (24–26), procaspase-3 was transiently overexpressed to elevate the expression levels of caspase-3, and the preparation of subcellular fractions was carried out in the presence of a proteasome inhibitor, lactacystin; PKC δ and lamin B1 were used as cytoplasmic and nuclear fraction markers, respectively. Normal non-transfected HepG2 cells (Fig. 1*B*, *left panel*) or transfected HepG2 cells treated with the anti-Fas antibody for 12 h (Fig. 1*B*, *right panel*) were fractionated into nuclear, membrane, and cytoplasmic fractions. Although the expression level of procaspase-3 in transfected cells was more than five times higher than in non-transfected cells, the cytoplasmic localization of procaspase-3 was unaffected by overexpression. Both caspase-3-p17 and caspase-3-p12 were detected not only in the cytoplasmic fraction but also in the nuclear fraction even after treatment with 0.5% Nonidet P-40 (Fig. 1*B*, *right panel*). These results strongly suggested that active caspase-3 was present in the nuclei of apoptotic cells.

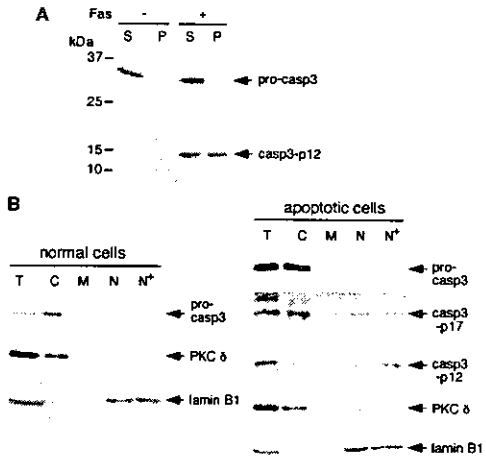

FIG. 1. **Nuclear localization of caspase-3-p17 and caspase-3-p12 subunits in apoptotic HepG2 cells.** *A*, detection of caspase-3-p12 subunit in HepG2 cells. HepG2 cells were treated with or without the anti-Fas antibody in the presence of actinomycin D for 12 h, and pellet (*P*) and supernatant (*S*) fractions were prepared after lysis with digitonin. Each fraction was subjected to SDS-PAGE and immunoblotted with anti-caspase-3 polyclonal antibodies (sc-1224 from Santa Cruz Biotechnology), which detect both procaspase-3 and caspase-3-p12. *B*, subcellular fractionation of normal (*left panel*) and apoptotic (*right panel*) HepG2 cells. Subcellular fractions from apoptotic HepG2 cells were prepared after transfection with pCAG-casp3 followed by incubation for 24 h and treatment with the anti-Fas antibody in the presence of actinomycin D for 12 h. Subcellular fractions, standardized to represent equal numbers of cells in each fraction, were subjected to SDS-PAGE and immunoblotted with anti-caspase-3 monoclonal antibody (C31720 from Transduction Laboratories), anti-caspase-3 antibody (9662 from Cell Signaling Technology), anti-caspase-3 polyclonal antibodies (sc-1224 from Santa Cruz Biotechnology), anti-PKC δ polyclonal antibodies, or anti-lamin B1 polyclonal antibodies. *T*, total cell lysate; *C*, cytoplasmic fraction; *M*, membrane fraction; *N*, purified nuclear fraction; N^+, purified nuclear fraction after treatment with 0.5% Nonidet P-40.

To directly assess the localization of active caspase-3, we prepared antibodies specific for active caspase-3-p12 subunit. Since procaspase-3 is processed at Asp^{28} and Asp^{175} sites to generate new N and C termini, we generated four affinity-purified polyclonal and three monoclonal antibodies that specifically recognize the newly exposed N-terminal region of caspase-3-p12 (see supplemental material). We also used the commercially available anti-active caspase-3 specific antibodies (G7481, Promega) that recognize the newly exposed C terminus of caspase-3-p17. Al-

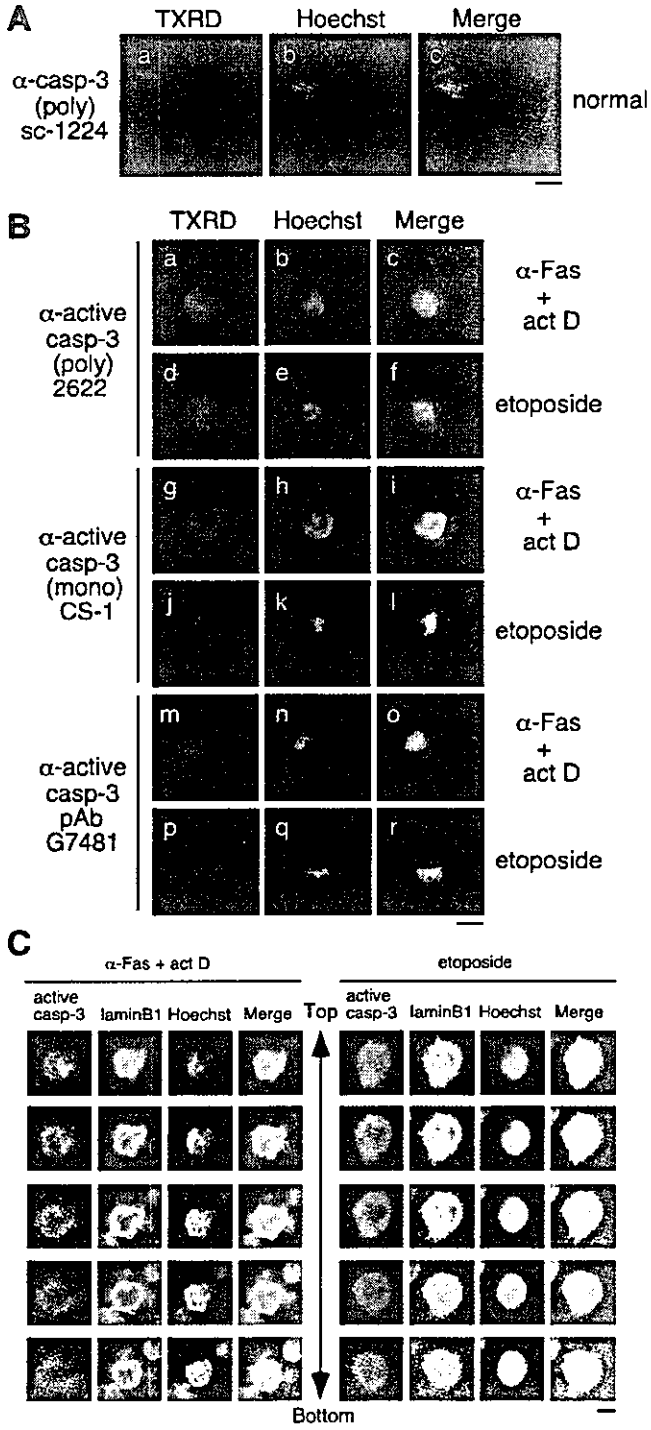

FIG. 2. **Nuclear accumulation of active caspase-3 in apoptotic cells.** *A*, cytoplasmic localization of procaspase-3 in normal cells. After fixation and permeabilization, HepG2 cells were incubated with anti-caspase-3 polyclonal antibodies (sc-1224 from Santa Cruz Biotechnology) and TXRD-labeled secondary antibodies (*panel a*), followed by staining the nuclei with Hoechst 33342 (*panel b*). Photographs were taken of the same fields in *panels a* and *b*, and merged images of TXRD and Hoechst staining are shown in *panel c*. *B*, accumulation of active caspase-3 around the apoptotic nuclei. HepG2 cells were treated with the anti-Fas antibody in the presence of actinomycin D (*act D*) for 12 h (*panels a–c, g–i,* and *m–o*) or with etoposide for 40 h (*panels d–f, j–l,* and *p–r*). After fixation and permeabilization, the cells were incubated with anti-active caspase-3 polyclonal antibodies (2622) (*panels a* and *d*), anti-active caspase-3 monoclonal antibody (CS-1) (*panels g* and *j*), anti-active caspase-3 pAb (G7481 from Promega) (*panels m* and *p*), and TXRD-labeled secondary antibodies (*panels a, d, g, j, m,* and *p*), followed by staining the nuclei with Hoechst 33342 (*panels b, e, h, k, n,* and *q*). Photographs were taken of the same fields in *panels a–c, d–f, g–i, j–l, m–o,* and *p–r*, and merged images of TXRD and Hoechst staining are shown in *panels c, f, i, l, o,* and *r*, respectively. *C*, detection of active caspase-3 in apoptotic nuclei. HepG2 cells were treated with the anti-Fas antibody in the presence of actinomycin D (*act D*) for 12 h or with etoposide for 40 h. After fixation and permeabilization, the cells were incubated with anti-active caspase-3 pAb (G7481 from Promega) and anti-lamin B1 polyclonal antibodies as a nuclear envelope marker, and Cy3- and Alexa Fluor 488-labeled secondary antibodies, followed by staining the nuclei with Hoechst 33342, and observed with confocal laser scanning microscope. The z-series of images from five sections are shown. *Bars*, 10 μm.

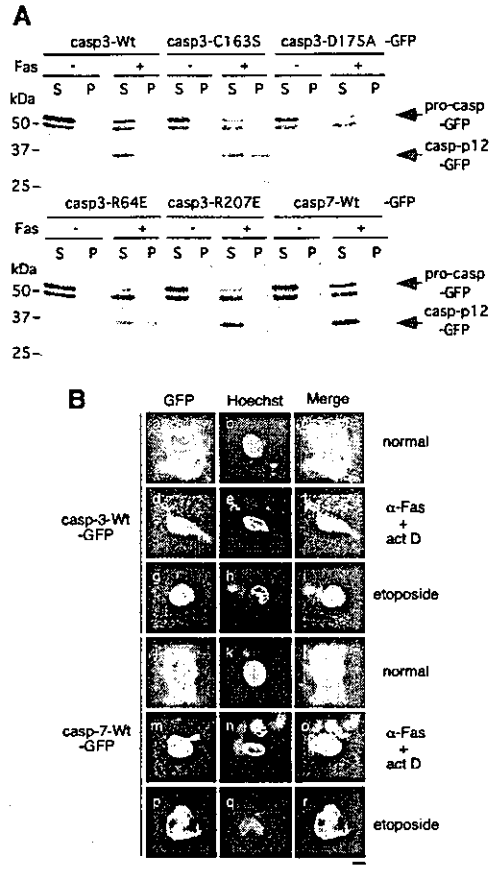

FIG. 3. **Nuclear translocation of active caspase-3 requires proteolytic activation and substrate recognition, but not catalytic activity.** *A*, localization of caspase-3- and caspase-7-GFP fusion proteins in HepG2 cells. One day before transfection, HepG2 cells were seeded at a density of 2×10^5 cells per well in 6-well dishes. In each well, 2 μg of plasmids expressing caspase-GFP fusion proteins were transfected and incubated for 24 h. After treatment with or without the anti-Fas antibody in the presence of actinomycin D (*act D*) for 12 h, cells were fractionated after lysis with digitonin and subjected to SDS-PAGE and immunoblotted with anti-GFP monoclonal antibody. *S*, supernatant fraction; *P*, pellet fraction. *B*, nuclear localization of caspase-3-, but not caspase-7-, GFP fusion protein in apoptotic cells with confocal laser scanning microscopy. One day before transfection, HepG2 cells were seeded at a density of 2×10^5 cells per 35-mm glass bottom dish. In each dish, 2 μg of pcasp3-Wt-GFP (*panels a–i*) or pcasp7-Wt-GFP (*panels j–r*) plasmids were transfected and incubated for 24 h. After treatment without (*panels a–c* and *j–l*) or with the anti-Fas antibody in the presence of actinomycin D (*act D*) for 12 h (*panels d–f* and *m–o*) or with etoposide for 40 h (*panels g–i* and *p–r*), GFP expression (*panels a, d, g, j, m,* and *p*) was observed with confocal laser scanning microscope after staining with Hoechst 33342 (*panels b, e, h, k, n,* and *q*). Photographs were taken of the same fields in *panels a–c, d–f, g–i, j–l, m–o,* and *p–r*, and merged images of GFP and Hoechst staining are shown in *panels c, f, i, l, o,* and *r*, respectively. *Bar*, 10 μm.

though procaspase-3 was detected in the cytoplasm of untreated normal cells (Fig. 2*A*), in most apoptotic cells stained with anti-active caspase-3 antibodies, which recognize the newly exposed N terminus of caspase-3-p12 (Fig. 2*B*, *panels a–l*) or the newly exposed C terminus of caspase-3-p17 (Fig. 2*B*, *panels m–r*), the signal was strongest around the condensed nucleus. To deter-

mine whether active caspase-3 is actually present in the nucleus, apoptotic cells were stained with the anti-active caspase-3 antibodies and antibodies against lamin B1, a nuclear envelope marker, and analyzed by confocal laser scanning microscopy (Fig. 2*C*). The signal for active caspase-3 was detected both in and around the condensed nuclei. Taken together, these results indicate that active caspase-3 is present not only in the cytoplasm but also in the nuclei of apoptotic cells.

To examine the molecular mechanisms governing translocation of caspase-3 from the cytoplasm into the nucleus, we constructed various procaspase-3 mutants fused with GFP. These constructs were transiently transfected into HepG2 cells. After treatment with or without the agonistic anti-Fas antibody to induce apoptosis, supernatant and pellet fractions were prepared after digitonin lysis and immunoblotted with the anti-GFP antibody (Fig. 3*A*). Although casp3-Wt-GFP was predominantly present in supernatant, like the unprocessed form before Fas treatment, proteolytically activated casp3-p12-GFP was recovered in both the supernatant and pellet fractions after Fas treatment (Fig. 3*A*). In contrast, caspase-7, another effector caspase, did not translocate to the nucleus, with both casp7-Wt-GFP and casp7-p12-GFP being detected only in the supernatant fraction irrespective of Fas treatment. Consistently, confocal laser scanning microscopy indicated that casp3-Wt-GFP was present in both cytoplasm and nuclei, whereas casp7-Wt-GFP was found only in the cytoplasm in apoptotic cells (Fig. 3*B*). These results suggested that the nuclear translocation of effector caspases is specific for caspase-3 and that the nuclear translocation of caspase-3 is an active process and not simply entail diffusion after disruption of the nuclear-cytoplasmic barrier.

To determine whether caspase-3 activation is needed for nuclear translocation, we constructed procaspase-3 mutants that cannot be activated, recognize substrates, or cleave substrates, respectively. Casp3-D175A-GFP, which is not activated due to mutation of the cleavage site between the p17 and p12 subunits, did not translocate after anti-Fas treatment, suggesting that the proteolytic activation of caspase-3 is necessary for its nuclear translocation (Fig. 3*A*). The three-dimensional structure of caspase-3 (27, 28) shows that Arg^{64} and Arg^{207} are essential for recognition of the P1 and P3 amino acids of the *DXXD* cleavage motif substrates, respectively. Cell fractionation analysis showed that casp3-R64E-GFP, but not casp3-R207E-GFP, translocated from cytoplasm to nuclei after Fas treatment, indicating that recognition of P3, but not P1, of a substrate(s) is necessary for nuclear translocation of active caspase-3 (Fig. 3*A*). Furthermore, casp3-C163S-GFP, in which the catalytic Cys is mutated, translocated from the cytoplasm into nuclei, indicating that substrate cleavage by caspase-3 is not essential for the translocation of active caspase-3. These results suggested that proteolytic activation and substrate recognition, but not substrate cleavage, are necessary for the nuclear translocation of active caspase-3.

Nuclear pore complexes (NPCs) mediate bidirectional transport between the cytoplasm and the nucleus (29). The NPC constitutes a passive diffusion channel, which allows the diffusion of ions, metabolites, and small proteins whose relative molecular mass is less than about 40 kDa. Proteins above the size limit can enter the nucleus by energy-dependent mechanisms. Caspase-3 lacks a typical consensus nuclear localization signal, and the active caspase-3 tetramer is too big to enter the nucleus passively. Recently, Faleiro and Lazebnik (16) reported that caspase-9 inactivates nuclear transport and increases the diffusion limit of the nuclear pore, leading to the entrance of caspase-3 into nuclei by diffusion. If caspase-3 enters the nucleus by simple diffusion, procaspase-3 as well as active caspase-3 and other caspases including caspase-7 would also be detected in the nuclear fraction of apoptotic cells. However, our data showed that neither procaspase-3 nor caspase-7 translocated into nuclei after apoptosis induction. Furthermore, active nuclear transport is required for the nuclear morphological changes induced by various apoptotic stimuli (30), and nuclear translocation of active caspase-3 required proteolytic activation and recognition of substrate-like protein(s). Therefore, we propose that the nuclear translocation of active caspase-3 is dependent on active nuclear transport. Identification of the substrate-like protein(s) which function as a carrier protein to transport active caspase-3 from the cytoplasm into nucleus in apoptotic cells is needed to clear the molecular mechanisms of nuclear translocation of active caspase-3.

Acknowledgments—We thank Drs. Yoshiteru Kobayashi and Shinji Tanahashi (Wako Pure Chemical Industries, Osaka, Japan) for cooperation in generating antibodies, Dr. Jeong-Hwa Lee for technical support in immunofluorescence analysis, Drs. Joel D. Leverson and Han-Kuei Huang for critical reading of the manuscript, Dr. Vishva M. Dixit for the pcDNA3/Yama plasmid, and Dr. Jun-ichi Miyazaki for the pUC-CAGGS plasmid.

REFERENCES

1. Alnemri, E. S., Livingston, D. J., Nicholson, D. W., Salvesen, G., Thornberry, N. A., Wong, W. W., and Yuan, J. (1996) *Cell* **87,** 171
2. Cryns, V., and Yuan, J. (1998) *Genes Dev.* **12,** 1551–1570
3. Thornberry, N. A., and Lazebnik, Y. (1998) *Science* **281,** 1312–1316
4. Earnshaw, W. C., Martins, L. M., and Kaufmann, S. H. (1999) *Annu. Rev. Biochem.* **68,** 383–424
5. Fernandes-Alnemri, T., Litwack, G., and Alnemri, E. S. (1994) *J. Biol. Chem.* **269,** 30761–30764
6. Tewari, M., Quan, L. T., O'Rourke, K., Desnoyers, S., Zeng, Z., Beidler, D. R., Poirier, G. G., Salvesen, G. S., and Dixit, V. M. (1995) *Cell* **81,** 801–809
7. Nicholson, D. W., Ali, A., Thornberry, N. A., Vaillancourt, J. P., Ding, C. K., Gallant, M., Gareau, Y., Griffin, P. R., Labelle, M., Lazebnik, Y. A., Mungay, N. A., Raju, S. M., Smulson, M. E., Yamin, T.-T., Yu, Y. L., and Miller, D. K. (1995) *Nature* **376,** 37–43
8. Kuida, K., Zheng, T. S., Na, S., Kuan, C., Yang, D., Karasuyama, H., Rakic, P., and Flavell, R. A. (1996) *Nature* **384,** 368–372
9. Woo, M., Hakem, R., Soengas, M. S., Duncan, G. S., Shahinian, A., Kagi, D., Hakem, A., McCurrach, M., Khoo, W., Kaufman, S. A., Senaldi, G., Howard, T., Lowe, S. W., and Mak, T. W. (1998) *Genes Dev.* **12,** 806–819
10. Zheng, T. S., Schlosser, S. F., Dao, T., Hingorani, R., Crispe, I. N., Boyer, J. L., and Flavell, R. A. (1998) *Proc. Natl. Acad. Sci. U. S. A.* **95,** 13618–13623
11. Enari, M., Sakahira, H., Yokoyama, H., Okawa, K., Iwamatsu, A., and Nagata, S. (1998) *Nature* **391,** 43–50
12. Liu, X., Li, P., Widlak, P., Zou, H., Luo, X., Garrard, W. T., and Wang, X. (1998) *Proc. Natl. Acad. Sci. U. S. A.* **95,** 8461–8466
13. Sahara, S., Aoto, M., Eguchi, Y., Imamoto, N., Yoneda, Y., and Tsujimoto, Y. (1999) *Nature* **401,** 168–173
14. Lechardeur, D., Drzymala, L., Sharma, M., Zylka, D., Kinach, R., Pacia, J., Hicks, C., Usmani, N., Rommens, J. M., and Lukacs, G. L. (2000) *J. Cell Biol.* **150,** 321–334
15. Fischer, U., Janicke, R. U., and Schulze-Osthoff, K. (2003) *Cell Death Differ.* **10,** 76–100
16. Faleiro, L., and Lazebnik, Y. (2000) *J. Cell Biol.* **151,** 951–959
17. Niwa, H., Yamamura, K., and Miyazaki, J. (1991) *Gene (Amst.)* **108,** 193–199
18. Martins, L. M., Mesner, P. W., Kottke, T. J., Basi, G. S., Sinha, S., Tung, J. S., Svingen, P. A., Madden, B. J., Takahashi, A., McCormick, D. J., Earnshaw, W. C., and Kaufmann, S. H. (1997) *Blood* **90,** 4283–4296
19. Mandal, M., Adam, L., and Kumar, R. (1999) *Biochem. Biophys. Res. Commun.* **260,** 775–780
20. Takemoto, K., Nagai, T., Miyawaki, A., and Miura, M. (2003) *J. Cell Biol.* **160,** 235–243
21. Thornberry, N. A., Rano, T. A., Peterson, E. P., Rasper, D. M., Timkey, T., Garcia-Calvo, M., Houtzager, V. M., Nordstrom, P. A., Roy, S., Vaillancourt, J. P., Chapman, K. T., and Nicholson, D. W. (1997) *J. Biol. Chem.* **272,** 17907–17911
22. Garcia-Calvo, M., Peterson, E. P., Leiting, B., Ruel, R., Nicholson, D. W., and Thornberry, N. A. (1998) *J. Biol. Chem.* **273,** 32608–32613
23. Zhivotovsky, B., Samali, A., Gahm, A., and Orrenius, S. (1999) *Cell Death Differ.* **6,** 644–651
24. Huang, H., Joazeiro, C. A., Bonfoco, E., Kamada, S., Leverson, J. D., and Hunter, T. (2000) *J. Biol. Chem.* **275,** 26661–26664
25. Suzuki, Y., Nakabayashi, Y., and Takahashi, R. (2001) *Proc. Natl. Acad. Sci. U. S. A.* **98,** 8662–8667
26. Chen, L., Smith, L., Wang, Z., and Smith, J. B. (2003) *Mol. Pharmacol.* **64,** 334–345
27. Rotonda, J., Nicholson, D. W., Fazil, K. M., Gallant, M., Gareau, Y., Labelle, M., Peterson, E. P., Rasper, D. M., Ruel, R., Vaillancourt, J. P., Thornberry, N. A., and Becker, J. W. (1996) *Nat. Struct. Biol.* **3,** 619–625
28. Wei, Y., Fox, T., Chambers, S. P., Sintchak, J., Coll, J. T., Golec, J. M. C., Swenson, L., Wilson, K. P., and Charifson, P. S. (2000) *Chem. Biol.* **7,** 423–432
29. Gorlich, D., and Mattaj, I. W. (1996) *Science* **271,** 1513–1518
30. Yasuhara, N., Eguchi, Y., Tachibana, T., Imamoto, N., Yoneda, Y., and Tsujimoto, Y. (1997) *Genes Cells* **2,** 55–64

ELSEVIER

European Journal of Cardio-thoracic Surgery 27 (2005) 117-121

EUROPEAN JOURNAL OF CARDIO-THORACIC SURGERY

www.elsevier.com/locate/ejcts

BH4 peptide derivative from Bcl-xL attenuates ischemia/reperfusion injury thorough anti-apoptotic mechanism in rat hearts

Masamichi Ono[a], Yoshiki Sawa[a,*], Masahiro Ryugo[a], Alexei N. Alechine[a], Shigeomi Shimizu[b], Rie Sugioka[b], Yoshihide Tsujimoto[b], Hikaru Matsuda[a]

[a]Department of Surgery, Osaka University Graduate School of Medicine, 2-2 Yamadaoka, Suita, Osaka 565-0871, Japan
[b]Department of Post-Genomics and Diseases, Osaka University Graduate School of Medicine, 2-2 Yamadaoka, Suita, Osaka 565-0871, Japan

Received 18 May 2004; received in revised form 6 September 2004; accepted 9 September 2004

Abstract

Objective: To prevent apoptosis is thought to be promising for myocardial protection in cardiac surgery. Recently, we showed that BH4 domain of Bcl-xL is essential for the prevention of apoptosis, and that BH4 fused to HIV TAT protein (TAT-BH4) prevented apoptotic cell death. Then, we hypothesized TAT-BH4 may attenuate ischemia/reperfusion injury in rat hearts. **Methods**: The isolated rat hearts in the TAT-BH4 preconditioning group (BH4 group, $n=8$) or control group (C group, $n=8$) were subjected to warm ischemia (37 °C) for 30 min followed by 60 min of reperfusion using Langendorff perfusion system. **Results**: Left ventricular developed pressure and maximum dP/dt after reperfusion were significantly improved in the BH4 group than those in the C group ($P<0.01$). Recovery of mitochondrial respiration was significantly better in the BH4 group ($P<0.05$). Moreover, expression of caspase-3 and TUNEL-positive myocardium were decreased in the BH4 group than those in the C group. **Conclusions**: These results demonstrated that TAT-BH4 attenuates myocardial ischemia/reperfusion injury through preventing myocardial apoptosis. Thus, TAT-BH4 may be a novel therapeutic agent for myocardial protection in cardiac surgery.

Keywords: Apoptosis; Cardiomyocytes; Ischemia/reperfusion injury; Heart surgery

1. Introduction

Recent advances in myocardial protection have improved the clinical results in open-heart surgery. However, severely critical cases associated with compromised heart, such as failing heart or post-ischemic conditions, still occur, and thus, further attempts to improve myocardial protection should be addressed.

Recently, a growing body of evidence have shown that apoptosis of myocardium is one of the major contributors to ischemic/reperfusion injury in experimental models [1-5] and even in humans after open-heart surgery [6,7]. Therefore, many attempts through molecular mechanism to attenuate apoptosis of myocardium in ischemia/reperfusion injury have been reported [8-15]. However, no pharmacological strategy has been reported to attenuate apoptosis in the heart. Moreover, strategy using gene transfection during ischemia has limitations because it takes few ours to express proteins after reperfusion, which is not suitable for clinical application of myocardial protection against acute ischemic reperfusion injury.

We recently demonstrated that the biochemical role of the conserved N-terminal homology domain (BH4) of Bcl-xL is essential for the prevention of apoptosis, with respect to the regulation of mitochondrial membrane permeability and found that BH4 was required for Bcl-xL to prevent cytochrome *c* release. Using a newly developed TAT protein transduction system, which is the protein transduction domain of human immunodeficiency virus type 1 Tat protein (HIV TAT protein), we also showed that the BH4 domain fused to TAT protein (TAT-BH4), effectively prevented apoptotic cell death in vitro [16], and showed feasibility of protein transduction into cells in vivo. Chen et al. demonstrated TAT-BH4 attenuated myocardial infarction in vivo [17]. Therefore, it is expected that preconditioning of TAT-BH4 may attenuate ischemia/reperfusion injury of the myocardium during open heart surgery.

In this study, we investigated whether the preconditioning of TAT-BH4 may attenuate ischemia/reperfusion injury in isolated rat heart model as a pre-clinical trial.

* Corresponding author. Tel.: +81 6 6879 3151; fax: +81 6 6879 3163.
E-mail address: sawa@surg1.med.osaka-u.ac.jp (Y. Sawa).

1010-7940/$ - see front matter © 2004 Elsevier B.V. All rights reserved.
doi:10.1016/j.ejcts.2004.09.025

2. Method

2.1. Test compounds

TAT-BH-4 protein and TAT mutant protein were provided by Shionogi Pharmacy Co., Ltd, Osaka, Japan. The proteins were dissolved in DMSO to the concentration of 5 μg/μl before use.

2.2. Pharmacological preconditioning and rat ischemia model

Sixteen Sprague-Dawley rats (300 g, male) were used for this study. Humane animal care complied with the 'Principle of Laboratory Animal Care' formulated by the National Society for Medical Research and the 'Guide for the Care and Use of Laboratory Animals' prepared by the Institute of Laboratory Animal Resource and published by the Institutes of Health (NIH Publication No. 86-23, revised 1985). The rats were divided into the control group (C group, $n=8$), and the TAT-BH-4 group (BH4 group, $n=8$). All rats were anesthetized by intra-peritoneal injection of sodium pentobarbital (50 mg/kg). Following 10 min of the injection and anticoagulation with heparin (200 USP units, intra-peritoneally), the hearts were quickly excised and perfused with modified Krebs-Henseleit buffer (120.0 mM NaCl, 4.5 mM KCl, 20.0 mM $NaHCO_3$, 1.2 mM KH_2PO_4, 1.2 mM $MgCl_2$, 2.5 mM $CaCl_2$, and 10.0 mM glucose: gassed with 95% O_2+5% CO_2 to obtain pH 7.4 at 37 °C) at the pressure equal to 1 m H_2O by means of a Langendorff apparatus. A thin-wall latex balloon was inserted into the left ventricle through the left atrium to monitor left ventricular pressure and to control left ventricular volume. After stabilization, heart rate (HR), left ventricular developed pressure (LVDP), maximum dP/dt (max dP/dt), and coronary flow (CF) were measured with LV diastolic pressure stabilized at 10 mmHg. Then, 100 μg (20 μl) of TAT-BH4 protein (BH4 group) or TAT mutant protein (C group), diluted by 5 ml of modified Krebs-Henseleit buffer, were administered through side port of apparatus at the speed of 1 ml/min. The hearts were then subjected to global ischemia at 37 °C for 30 min, followed by 60 min of reperfusion. The balloon was deflated during ischemia. The indices of cardiac function were continuously measured after reperfusion and analyzed using Polygraph System (Nihon Kouden, Japan). After 60 min of reperfusion, frozen sections of the hearts were made and stored at −80 °C for further assessment.

2.3. The recovery of mitochondrial respiration

Mitochondria were isolated from the hearts after reperfusion in 0.3 M mannitol/10 mM potassium Hepes, pH 7.4/0.2 mM EGTA, pH 7.4/0.1% fatty acid-free BSA by centrifugation at 2500×g for 10 min. The mitochondria were washed twice with this medium without EGTA to which 5 mM potassium phosphate was added and then suspended in it. Mitochondrial respiration was measured with an O_2 electrode, and the recovery of respiration was defined as the ratio of mitochondrial respiration in the hearts after reperfusion to the hearts before ischemia.

2.4. Western blotting analysis of active caspase-3

To evaluate the activation of apoptotic cascade after reperfusion, western blot analysis for detection of active caspase-3 was performed using the frozen section samples after 60 min of reperfusion. We used active caspase-3 rabbit polyclonal IgG antibody, and anti-rabbit secondary antibody conjugated to horseradish peroxidase and Phototope-HRP Western detection kit. The degree of the protein expression was semi-quantitatively evaluated with computed densitometry (Scion Image: Windows; Microsoft Corporation).

2.5. Histological analysis of apoptosis

The frozen section samples after 60 min of reperfusion were prepared for histological analysis. TUNEL staining was performed using Terminal Deoxynucleotidyle Transferase Mediated UTP-Biotin In Situ Nick-End Labeling (Tunnel Intergen Kit) according to the manufacturer's instruction. Quantitative assessment was calculated as a percentage of TUNEL-positive nuclei.

2.6. Statistical analysis

All data are expressed as mean±standard error of the means (SEM). Scores were compared using an unpaired Student's t test. A P value of less than 0.05 was considered statistically significant.

3. Results

3.1. Recovery of cardiac function after global ischemia

To evaluate the efficacy of TAT-BH4 protein, we firstly analyzed cardiac function after global warm ischemia and reperfusion. The time course of percent recovery of LVDP after global ischemia (37 °C, 30 min) was shown in Fig. 1A. In comparison with the C group, a significant improvement of the percent recovery of LVDP was observed in the BH4 group at 10, 20, 30, 40, 50, and 60 min after reperfusion. The value after 60 min of reperfusion in the C group was 47±4%, and was significantly improved to 72±4% in the BH4 group ($P<0.01$).

The time course of percent recovery of max dP/dt after global ischemia was shown in Fig. 1B. In comparison with the C group, a significant improvement of the index was observed in the BH4 group at 20, 30, 40, 50, and 60 min after reperfusion. The value after 60 min of reperfusion in the C group was 36±9%, and was significantly improved to 71±3% in the BH4 group ($P<0.01$). CF after 60 min reperfusion was also significantly higher in the BH4 group compared with the C group (13.8±0.9 vs. 8.9±1.2 ml/min; $P<0.01$) (Fig. 1C).

3.2. Mitochondrial function by the recovery of respiration

Consistently, mitochondrial function assessed by the recovery of respiration markedly increased (C; 30±5, B; 77±10%, $P<0.05$) (Fig. 2).

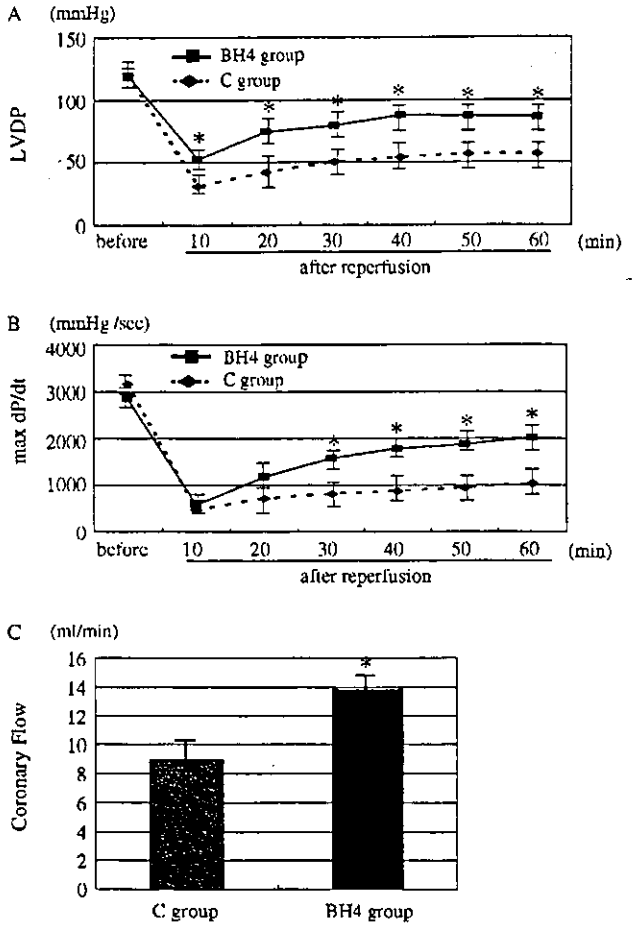

Fig. 1. Cardiac function after reperfusion. The isolated hearts from the two groups were subjected to 30 min of normothermic global ikschemia followed by 60 min of reperfusion. Better recovery of LVDP (A) and maximum dP/dt (B) after ischemia was shown in the BH4 group than in the C group. Data are expressed as percentage of basal value before ischemia. $^{**}P<0.01$, $^{*}P<0.05$. The coronary flow after reperfusion (C): the coronary flow 60 min after reperfusion was measured. $^{*}P<0.05$. $n=8$ in each group. All values are expressed as mean±SEM.

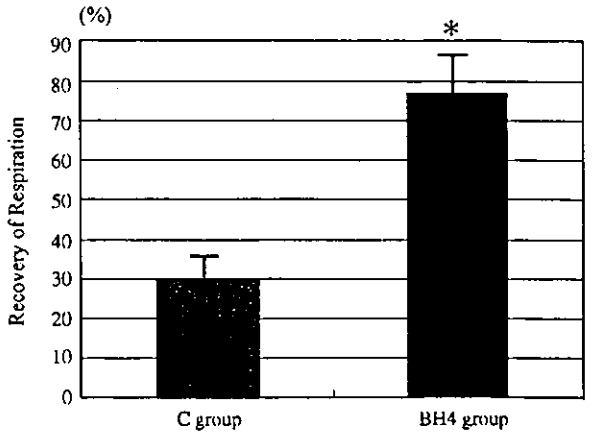

Fig. 2. The recovery of respiration: the recovery of mitochondrial respiration 60 min after reperfusion was measured. $^{*}P<0.05$. $n=8$. All values are expressed as mean±SEM.

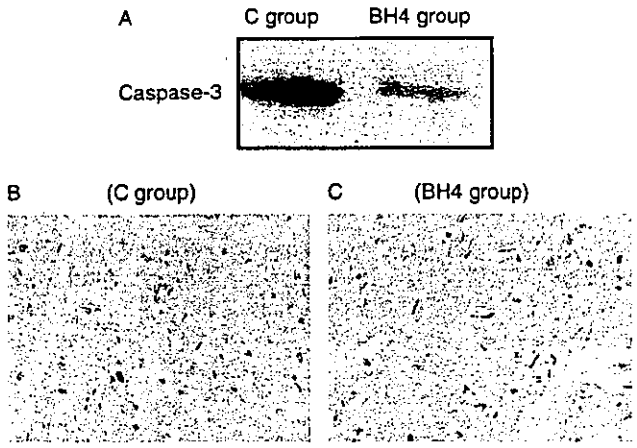

Fig. 3. Apoptosis of the myocardium after reperfusion. The myocardial expression of caspase-3 was significantly lower in the BH4 group than in the C group (A). The TUNEL-positive cardiomyocytes has detected in the control (B), but not in the BH4 group (C).

3.3. Evaluation of apoptosis by active caspase-3 expression and TUNEL staining

Then, we evaluated the apoptosis of the myocardium by Western blotting of active caspase-3 and TUNEL staining of the myocardium 60 min after reperfusion. The western blotting analysis for caspase-3 showed lower expression of active caspase-3 in the BH4 group compared with the C group (Fig. 3A). According to semi-quantitative analysis with computed densitometry, the BH4 group showed 1/3-1/4 less caspase-3 expression than the C group. The TUNEL staining of the heart section showed none of TUNEL-positive cells in the BH4 group (Fig. 3C), but significantly positive in the C group (Fig. 3B). The percent TUNEL-positive cells in the C group was 2.2±0.3% of all cardiomyocytes, whereas TUNEL-positive cells could not be seen in BH4 group ($P<0.01$).

4. Discussion

In the present report, we showed cardioprotective effect of TAT-BH4; a novel linkage of the protein transduction domain of HIV TAT to the functional domain of Bcl-xL. The recovery of cardiac function, mitochondrial respiration of the myocardium after ischemia/reperfusion was significantly better by TAT-BH4 administration. Moreover, TAT-BH4 attenuated caspase-3 expression and reduced apoptosis of cardiomyocytes.

Apoptosis is an actively regulated process of cellular self-destruction, thereby distinct from necrosis. It encloses mitochondrial changes with characteristic release of substances promoting apoptosis like cytochrome *c*. Downstream in the apoptotic program the caspase cascade such as caspase-3 is activated, followed by cytoskeletal alterations, chromatin condensation, and DNA fragmentation, culminating in cell death. Previous experimental studies have well shown that apoptosis of cardiomyocytes is induced from early stage of ischemia/reperfusion, playing an important role for the cardiac dysfunction [1-5]. Using isolated rat

heart model, Scarabelli et al. [4] demonstrated that apoptosis (caspase-3 and TUNEL-positive nuclei) is seen in the very early stages (5 min of reperfusion) of ischemia/reperfusion in both endothelial cells and cardiomyocytes. Previous clinical studies also demonstrated apoptosis is evident early after ischemia/reperfusion during open-heart surgery. Schmitt et al. [6] showed that cytochrome *c* release and TUNEL-positive myocytes were increased even at the time of weaning from extracorporeal circulation (40 min of reperfusion), and apoptotic index showed a negative correlation with left ventricular function during surgery. Wu et al. [7] demonstrated percent TUNEL-positive myocytes was significantly increased even just after cross-claming release (10 min of reperfusion). These findings are consistent with our result of increased caspase-3 activities and TUNEL-positive myocytes 60 min after reperfusion.

There are many reports to attenuate ischemia/reperfusion injury through inhibiting apoptosis [8-15]. Several reports demonstrated the effects of gene transfer of anti-apoptotic gene [8-12]. Huang et al. [11] showed the effects of Bcl-xL gene transfer in rat model, but gene transfection needs a couple of days to gene expression, so this method is not suitable clinically for cardio-protection during open heart surgery. Other reports [13-15] showed the effects of anti-apoptotic protein administration such as caspase inhibitor [13], but this method needs frequent or continuous administration of relatively high dose of drugs during ischemia and reperfusion, which might induce deleterious side effects in other organs. Compared with the previous methods, TAT-BH4 administration before ischemia has some advantages over previous approach, because administration of essential domain for Bcl-xL by TAT system enables effective protein transduction into the target cells and potentiate immediately after reperfusion.

Our results showed that BH4 administration suppressed apoptotic cascade, resulting in improvement of cardiac function from early stage of reperfusion. Caspase-3 expression, an important molecule in the cellular suicide cascade, was minimal and no TUNEL-positive cells were seen in the BH4 group. The mechanism that BH4 inhibits apoptosis has already been demonstrated in our previous report [16]. BH4 of Bcl-xL is essential for inhibition of apoptosis with respect to the regulation of mitochondrial membrane permeability and is able to inhibit both voltage-dependent anion channel activity even in the presence of Bax and apoptotic mitochondrial membrane permeability loss. The mechanisms of this rapid effect for cardiac function by inhibiting apoptosis is remain to be addressed. Cheng et al. [18] reported that even such a small number of cells affected by apoptosis may have a significant impact on cardiac contractility, because single-cell death impinges upon the force-generating ability of neighboring cells that are still viable but stunned. Relatively few apoptotic cells may substantially impair side-to-side slippage of myocytes, resulting in a disproportionate and much more severe cardiac dysfunction. As a result, TAT-BH4 administration before ischemia inhibited almost completely apoptotic cascade during ischemia/reperfusion, contributing improvement of cardiac function from the early stage of reperfusion.

The HIV TAT protein: the amino-acid transduction domain of TAT contains a domain that facilitates protein transduction across cellular membranes. Although the exact mechanism of protein transduction across cellular membranes remains unknown, TAT-mediated protein transduction has been shown to occur even at 4 °C and is receptor independent [19]. These characteristics of TAT protein are also thought to be promising for protein transduction during open heart surgery.

These well known mechanisms of TAT-BH4 preventing mitochondrial function and apoptosis characterizes the promising possibility for clinical appreciation of this agent in cardiac surgery. Our data have strongly supported the importance of further investigation for clinical appreciation of this agent in future.

In conclusion, we obtained evidence that TAT-BH4 attenuates myocardial ischemia/reperfusion injury via inhibition of apoptosis of the myocardium. Thus, TAT-BH4 may be a novel therapeutic strategy for the protection of post-operative cardiac dysfunction in cardiovascular surgery.

References

[1] Gill C, Mestril R, Samali A. Losing heart: the role of apoptosis in heart disease—a novel therapeutic target? Fed Am Soc Exp Biol J 2002;16:135-46.

[2] Freude B, Masters TN, Robicsek F, Fokin A, Kostin S, Zimmermann R, Ullmann C, Lorenz-Meyer S, Schaper J. Apoptosis is initiated by myocardial ischemia and executed during reperfusion. J Mol Cell Cardiol 2002;32:197-208.

[3] Vazquez-Jimenez JF, Qing M, Hermanns B, Klosterhalfen B, Woltje M, Chakupurakal R, Schumacher K, Messmer BJ, von Bernuth G, Seghaye MC. Moderate hypothermia during cardiopulmonary bypass reduces myocardial cell damage and myocardial cell death related to cardiac surgery. J Am Coll Cardiol 2001;38:1216-23.

[4] Scarabelli T, Stephanou A, Rayment N, Pasini E, Comini L, Curello S, Ferrari R, Knight R, Latchman D. Apoptosis of endothelial cells precedes myocyte cell apoptosis in ischemia/reperfusion injury. Circulation 2001;104:253-6.

[5] Gottlieb RA, Burleson KO, Kloner RA, Babior BM, Engler RL. Reperfusion injury induces apoptosis in rabbit cardiomyocytes. J Clin Invest 1994;94:1621-8.

[6] Schmitt JP, Schroder J, Schunkert H, Birnbaum DE, Aebert H. Role of apoptosis in myocardial stunning after open heart surgery. Ann Thrac Surg 2002;73:1229-35.

[7] Wu ZK, Laurikka J, Saraste A, Kyto V, Pehkonen EJ, Savunen T, Tarkka MR. Cardiomyocyte apoptosis and ischemic preconditioning in open heart operations. Ann Thrac Surg 2003;76:528-34.

[8] Sawa Y, Morishita R, Suzuki K, Kagisaki K, Kaneda Y, Maeda K, Kadoba K, Matsuda H. A novel strategy for myocardial protection using in vivo transfection of cis element 'decoy' against NFκB binding site: evidence for a role of NFκB in ischemia/reperfusion injury. Circulation 1997;96(suppl):II-280-II-285.

[9] Suzuki K, Murtuza B, Smolenski RT, Sammut IA, Suzuki N, Kaneda Y, Yacoub MH. Overexoression of interleukin-1 receptor antagonist provides cardioprotection against ischemia-reperfusion injury associated with reduction in apoptosis. Circulation 2001;104(suppl I):I-308-I-313.

[10] Suzuki K, Murtuza B, Sammut IA, Latif N, Jayakumar J, Smolenski RT, Kaneda Y, Sawa Y, Matsuda H, Yacoub MH. Heat shock protein 72 enhances manganese superoxide dismutase activity during myocardial ischemia-reperfusion injury, associated with mitochondrial protection and apoptosis reduction. Circulation 2002;106(suppl):I-270-I-276.

[11] Huang J, Ito Y, Morikawa M, Uchida H, Kobune M, Sasaki K, Abe T, Hamada H. Bcl-xL gene transfer protects the heart against ischemia/reperfusion injury. Ann Thrac Surg 2002;73:1229-35.

[12] Kato K, Yin H, Agata J, Yoshida H, Chao L, Chao J. Adrenomedullin gene delivery aattenuates myocardial infarction and apoptosis after ischemia and reperfusion. Ann J Physiol Heart Circ Physiol 2003;285:H1506-H14.
[13] Yaoita H, Ogawa K, Maehara K, Maruyama Y. Attenuation of ischemia/reperfusion injury in rats by a caspase inhibitor. Circulation 1998;97: 276-81.
[14] Grunenfelder J, Miniati DN, Murata S, Falk V, Hoyt EG, Robbins RC. Upregulation of Bcl-2 through caspase-3 inhibition ameriolates ischemia/reperfusion injury in rat cardiac allografts. Circulation 2001; 104(suppl):I-202-I-206.
[15] Maejima Y, Adachi S, Ito H, Nobori K, Tamamori-Adachi M, Isobe M. Nitric Oxide inhibits ischemia/reperfusion-induced myocardial apoptosis by modulation cyclin A-associated kinase activity. Cardiovasc Res 2003;59: 308-20.
[16] Shimizu S, Konishi A, Kodama T, Tsujimoto Y. BH4 domain of antiapoptotic Bcl-2 family members closes voltage-dependent anion channel and inhibits apoptotic mitochondrial changes and cell death. Proc Natl Acad Sci USA 2000;97:3100-5.
[17] Chen M, Won DJ, Krajewski S, Gottlieb RA. Calpain and mitochondria in ischemia/reperfusion injury. J Biol Chem 2002; 277:29181-6.
[18] Cheng W, Li B, Kajstura J, Wolin MS, Sonnenblick EH, Hintze TH, Olivetti G, Anversa P. Stretch-induced programmed myocytes cell death. J Clin Invest 1995;96:2247-59.
[19] Gustafsson AB, Sayen MR, Williams SD, Crow MT, Gottlieb RA. TAT protein transduction into isolated perfused hearts: TAT-apoptosis represser with caspase recruitment domain is cardioprotective. Circulation 2002;106:735-9.

Cyclophilin D-dependent mitochondrial permeability transition regulates some necrotic but not apoptotic cell death

Takashi Nakagawa[1,2,4], Shigeomi Shimizu[1,4], Tetsuya Watanabe[3], Osamu Yamaguchi[3], Kinya Otsu[3], Hirotaka Yamagata[1], Hidenori Inohara[2], Takeshi Kubo[2] & Yoshihide Tsujimoto[1,4]

[1]*Laboratory of Molecular Genetics, Department of Post-Genomics and Diseases,* [2]*Department of Otolaryngology and Sensory Organ Surgery and* [3]*Department of Internal Medicine and Therapeutics, Osaka University Medical school, 2-2 Yamadaoka, Suita, Osaka 565-0871, Japan*

[4]*Solution-Oriented Research for Science and Technology (SORST), Japan Science and Technology Corporation, 2-2 Yamadaoka, Suita, Osaka 565-0871, Japan*

Mitochondria play an important role in energy production, Ca^{2+} homeostasis and cell death. In recent years, the role of the mitochondria in apoptotic and necrotic cell death has attracted much attention[1,2]. In apoptosis and necrosis, the mitochondrial permeability transition (mPT), which leads to disruption of the outer mitochondrial membrane and mitochondrial dysfunction, is considered to be one of the key events, although its exact role in cell death remains elusive. We therefore created mice lacking cyclophilin D (CypD), a protein considered to be involved in the mPT, to analyse its role in cell death. CypD-deficient mice were developmentally normal and showed no apparent anomalies, but CypD-deficient mitochondria did not undergo the cyclosporin A-sensitive mPT. CypD-deficient cells died normally in response to various apoptotic stimuli, but showed resistance to necrotic cell death induced by reactive oxygen species and Ca^{2+} overload. In addition, CypD-deficient mice showed a high level of resistance to ischaemia/reperfusion-induced cardiac injury. Our results indicate that the CypD-dependent mPT regulates some forms of necrotic death, but not apoptotic death.

The mitochondrial permeability transition (mPT) is a regulated Ca^{2+}-dependent increase in the permeability of the mitochondrial membrane, which results in a loss in mitochondrial membrane potential ($\Delta\Psi$) mitochondrial swelling and rupture of the outer membrane[3]. The mPT is thought to occur after the opening of a channel, termed the permeability transition pore, which putatively consists of a voltage-dependent anion channel, an adenine nucleotide translocator, CypD, and some other molecule(s)[4]; however, an essential role for the adenine nucleotide translocator in the mPT is a matter of recent controversy[5,6].

CypD is a mitochondrial member of the cyclophilin family of peptidyl prolyl-*cis*, *trans*-isomerases (PPIases) and has a crucial role in protein folding[7]. It has been suggested that CypD is involved in regulating the mPT, on the basis of the observation that cyclosporin A (CsA), a specific inhibitor of cyclophilin family activity, blocks the mPT[8]. A CsA-insensitive mPT has also been suggested, although the molecular mechanism is completely unknown[9]. It has been shown that some forms of apoptosis are significantly inhibited by CsA, suggesting a role for CsA-sensitive mPT in apoptosis[2,4]. The mPT is also implicated in the remodelling of mitochondrial structure with mobilization of cytochrome *c* stores in cristae during apoptosis[10]. To determine whether CypD has a crucial role in the CsA-sensitive mPT, and to investigate whether the mPT is a key regulator of cell death, we created CypD-deficient mice by gene targeting (see Supplementary Fig. 1a–c). The absence of cyclophilin D protein in CypD-deficient mice was verified by western blotting (see Fig. 1a and Supplementary Fig. 1d). CypD-deficient mice were born at the expected mendelian frequency, developed normally, and did not have any detectable phenotypic anomalies.

To examine the role of CypD in the mPT, mitochondria were isolated from the livers of CypD-deficient mice and control littermates. The mitochondria showed no significant change in respiration rate in the absence of CypD (see Supplementary Fig. 2). As shown in Fig. 1a, PPIase activity was absent in CypD-deficient mitochondria, but not in control mitochondria, indicating that CypD is the major PPIase in the mitochondria. When control mitochondria were treated with 50 μM Ca^{2+}, the mPT occurred, as shown by mitochondrial swelling (Fig. 1b) and loss of $\Delta\Psi$ (Fig. 1c). These phenomena were not observed in CypD-deficient mitochondria (Fig. 1b, c). To examine the extent of mPT inhibition as a consequence of CypD-deficiency, successive doses of Ca^{2+} were added to the mitochondria. $\Delta\Psi$ was lost after two additions of 50 μM Ca^{2+} to control mitochondria, but it was still maintained after seven additions of Ca^{2+} to CypD-deficient mitochondria (Fig. 1d). We investigated whether the absence of Ca^{2+}-induced mPT in CypD-deficient mitochondria was due to disturbance of Ca^{2+} uptake. As shown in Fig. 1e, the extra-mitochondrial Ca^{2+} concentration increased transiently, and rapidly returned to basal levels after each successive addition of Ca^{2+} to CypD-deficient mitochondria, indicating normal Ca^{2+} uptake by the mitochondria. Up to concentrations of 500 μM Ca^{2+}, most of the Ca^{2+} was taken up by CypD-deficient mitochondria (Fig. 1e, f). Next, we analysed CypD-deficient mitochondria in the presence of much higher concentrations of Ca^{2+}, which can induce CsA-insensitive mPT[9]. Addition of more than 1 mM Ca^{2+} induced swelling, collapse of $\Delta\Psi$, and impaired Ca^{2+} uptake even in CypD-deficient mitochondria (Fig. 1f and Supplementary Fig. 3), and all of these events were insensitive to CsA, even when it was added to CypD-deficient mitochondria (see Supplementary Fig. 3). Taken together, these results suggest that the mPT induced by low doses of Ca^{2+} is completely inhibited in CypD-deficient mitochondria, and that CypD is not involved in the CsA-insensitive increase in membrane permeability induced by high doses of Ca^{2+}. Furthermore, the addition of other mPT inducers, such as H_2O_2 and atractyloside, did not trigger the mPT in CypD-deficient mitochondria (see Supplementary Fig. 4).

In many forms of apoptosis, BH3-domain-containing proteins of the Bcl-2 family ('BH3-only' proteins) transduce apoptotic signals to the mitochondria, and induce cytochrome *c* release in a Bax/Bak-dependent manner[11]. Whether the CsA-sensitive mPT is involved in apoptotic cytochrome *c* release is controversial[12–15]. To address this question, we added recombinant Bid (rBid), one of the BH3-only proteins, to CypD-deficient and control mitochondria. As shown in Fig. 1g (top panel), CypD deficiency had no effect on rBid-induced cytochrome *c* release, which was different from the result in Bak-deficient mitochondria (Fig. 1g, bottom panel). Bad (another BH3-only protein, data not shown) and rBax (Fig. 1g; second panel), were also found to induce cytochrome *c* release equally in both CypD-deficient and control mitochondria. In contrast, Ca^{2+}-induced cytochrome *c* release was markedly reduced in CypD-deficient mitochondria (Fig. 1g; third panel). Interestingly, Bak deficiency did not have any effect on Ca^{2+}-induced cytochrome *c* release (Fig. 1g, bottom panel). Together, these data indicate that the mPT is involved in cytochrome *c* release induced by Ca^{2+}, but not by pro-apoptotic BH3-only proteins or Bax.

The results described above raise the possibility that the mPT might be involved in cell death due to mPT inducers (including Ca^{2+} overload and reactive oxygen species), but is not involved in the common apoptotic pathway to which BH3-only proteins and Bax/Bak are committed. We first examined the responses of CypD-deficient cells to these death stimuli. As shown in Fig. 2a, control and CypD-deficient thymocytes underwent comparable levels of apoptosis when exposed to various apoptotic stimuli. Similar findings were also obtained when murine embryonic fibroblast cells (MEFs) and hepatocytes from CypD-deficient mice

letters to nature

were treated with various apoptotic reagents (Fig. 2b, c), and when these cells were transfected with DNA encoding Bax or a truncated form of Bid (tBid; Fig. 2d, e). Moreover, apoptotic death of intestinal epithelial cells also occurred equally in control and CypD-deficient mice subjected to X-ray irradiation (Fig. 2f). These results indicate that CypD-dependent (CsA-sensitive) mPT is not involved in the common apoptotic pathway.

Next, we tested control and CypD-deficient MEFs for cell death after exposure to H_2O_2. CypD-deficient MEFs were more resistant to H_2O_2-induced cell death than control cells as assessed by a CTB (cell titre blue) assay, which measures the metabolic activity of viable cells (Fig. 3a), and by Annexin-V staining (data not shown). H_2O_2-induced cell death is predominantly due to necrosis, based on the following observations: a lack of caspase activation (Fig. 3b), no effect of a caspase inhibitor (Fig. 3a), early disruption of the plasma membrane (Fig. 3c), and finally, no nuclear or oligonucleosomal DNA fragmentation (Fig. 3c and data not shown). Similar results for H_2O_2-induced cell death were also obtained using CypD-deficient hepatocytes (Fig. 3d and data not shown).

We also examined the effect of CypD on cell death induced by A23187, a Ca^{2+} ionophore. CypD-deficient hepatocytes showed significant resistance to A23187-induced cell death (Fig. 3e). Like H_2O_2-induced cell death, A23187-induced cell death was not accompanied by caspase activation (Fig. 3f), so this type of

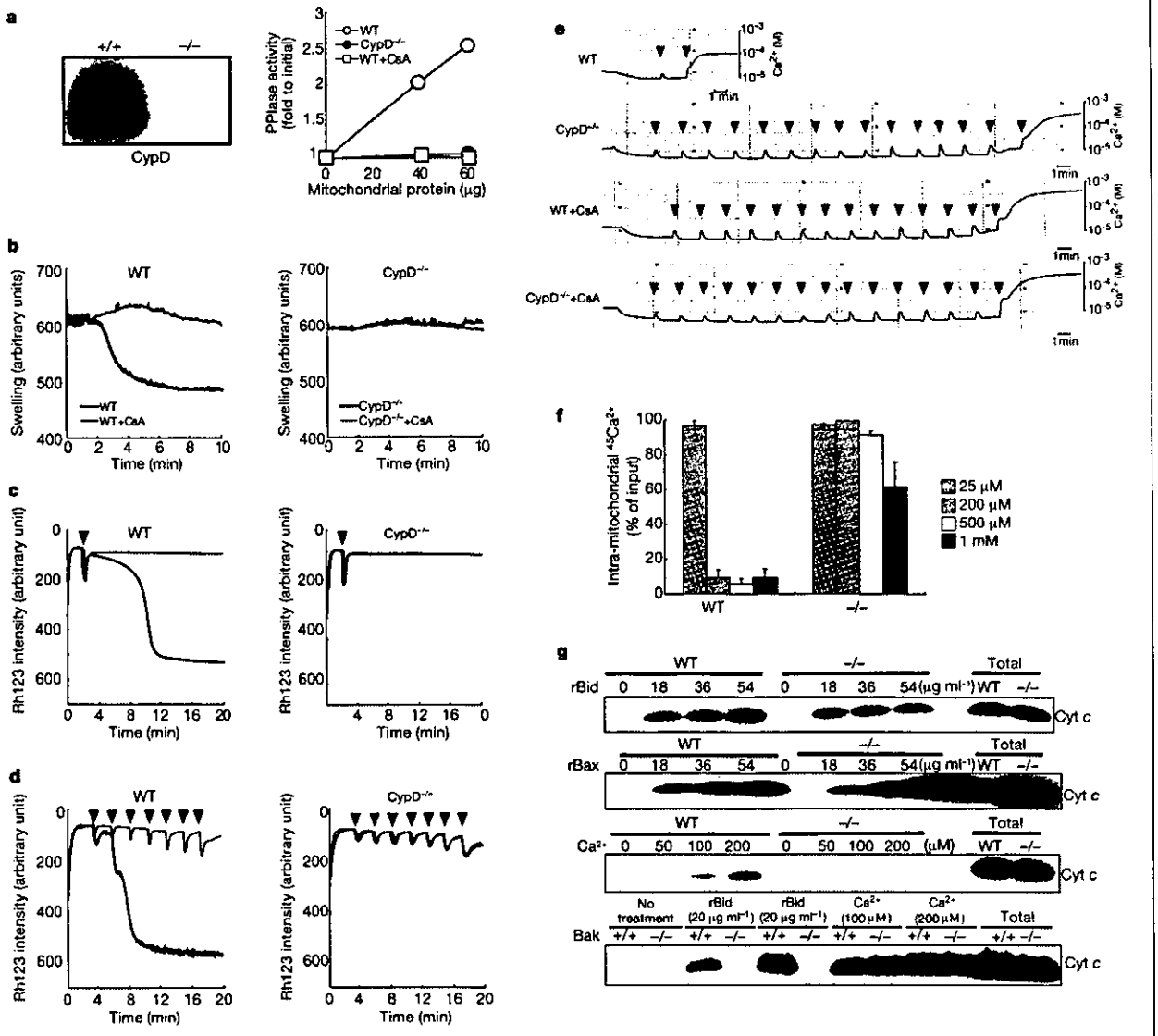

Figure 1 Absence of mPT in CypD-deficient ($CypD^{-/-}$) mitochondria. **a**, Absence of CypD protein and PPIase activity in Cyp $D^{-/-}$ mitochondria. WT, wild type. **b**, **c**, Absence of mPT in $CypD^{-/-}$ mitochondria. Isolated wild-type (WT, left column) or $CypD^{-/-}$ (right column) mitochondria were incubated with 50 μM Ca^{2+} in the presence (pink) or absence (blue) of 1 μM CsA, and monitored for (**b**) swelling (by light scatter) or (**c**) $\Delta\Psi$ (by Rh123 intensity), see Methods. Loss of $\Delta\Psi$ causes release of Rh123 from the mitochondria, resulting in increased Rh123 intensity. **d**, **e**, CypD deficiency prevents Ca^{2+}-induced $\Delta\Psi$ loss without altering Ca^{2+} uptake. Isolated mitochondria were successively treated with 50 μM Ca^{2+} (indicated by arrowheads) in the presence (pink) or absence (blue) of 1 μM CsA, and $\Delta\Psi$ (**d**) and extra-mitochondrial Ca^{2+} (**e**) were monitored. **f**, Accumulation of Ca^{2+} in the mitochondria as a result of CypD deficiency. Mitochondria were incubated with the indicated concentrations of $^{45}Ca^{2+}$ for 25 min and intra-mitochondrial Ca^{2+} was measured. Data shown as mean ± s.e.m. **g**, Lack of Ca^{2+}-induced, but not rBid- and rBax-induced, cytochrome *c* release in $CypD^{-/-}$ mitochondria. WT, $Bak^{-/-}$ and $CypD^{-/-}$ mitochondria were incubated with Ca^{2+}, rBid, and rBax at the indicated concentrations. After 30 min, samples were centrifuged and aliquots of supernatants were subjected to western blot analysis for cytochrome *c*. 'Total' represents the total amount of cytochrome *c* found in an equivalent aliquot of the mitochondria.

NATURE | doi:10.1038/nature03317 | www.nature.com/nature

death was also considered to represent necrotic cell death. These results indicate that CypD (and the CsA-sensitive mPT) is involved in necrotic cell death induced by oxygen radicals or Ca^{2+} overload.

Suppression of A23187-induced cell death by CypD deficiency seemed likely to be due to inhibition of the mPT. To determine whether A23187-induced mPT is suppressed by CypD deficiency in cells, we monitored mitochondrial $\Delta\Psi$ and Ca^{2+} accumulation in the presence of A23187. Hepatocytes were loaded with the $\Delta\Psi$ markers tetramethylrhodamine methylester (TMRM) or Mito Tracker Orange CMTM Ros, and treated with A23187, after which the fluorescence intensity was monitored by real-time imaging. Addition of A23187 caused rapid loss of $\Delta\Psi$ in control (wild-type) hepatocytes, whereas CypD-deficient hepatocytes maintained $\Delta\Psi$ for much longer periods of time (Fig. 3g–i and Supplementary Fig. 5). The addition of CCCP (carbonyl cyanide m-chlorophenyl-hydrazone), a protonophore, completely dissipated $\Delta\Psi$. Mitochondrial accumulation of Ca^{2+} was investigated using Rhod2-AM[16]. After A23187 treatment, CypD-deficient hepatocytes showed a rapid increase in Rhod2 fluorescence intensity, but wild-type hepatocytes showed only a marginal increase (Fig. 3j–l). The validity of using Rhod2 as an indicator of mitochondrial Ca^{2+} under these conditions was confirmed using Ru360, an inhibitor of the mitochondrial calcium uniporter (Fig. 3l). These results indicate that compared to control hepatocytes, CypD-deficient hepatocytes absorb a larger amount of cytosolic Ca^{2+} into their mitochondria without loss of mitochondrial $\Delta\Psi$; this is consistent with the results obtained using isolated mitochondria, and suggests that A23187 induces CypD-dependent mPT in cells.

Finally, we investigated the role of CypD in ischaemia/reperfusion (I/R) injury, in which disturbance of Ca^{2+} homeostasis and generation of reactive oxygen species have been implicated[17]. Many reports have described a protective effect of CsA against I/R injury[18–21]. First, we investigated whether CypD-deficient mitochondria showed resistance to anoxia/reoxygenation-induced injury, which simulates I/R-induced injury *in vivo*. Isolated mitochondria from control and CypD-deficient mice were subjected to anoxia for 30 min, followed by reoxygenation. Control mitochondria, but not CypD-deficient mitochondria, showed loss of $\Delta\Psi$ (Fig. 4a), swelling (Fig. 4b), leakage of mitochondrial asparatate aminotransferase (mAST) (Fig. 4c), and a severe decrease in respiratory control rate (Fig. 4d), indicating that CypD-deficient mitochondria are more resistant to anoxia/reoxygenation injury than control mitochondria.

We next examined the effect of CypD on cardiac I/R injury, because the heart has high levels of CypD (see Supplementary Fig. 1d). Several functional parameters assessed by echocardiography showed no differences between the resting hearts of control and CypD-deficient mice (see Supplementary Table). Mice were then subjected to 30 min of left coronary artery occlusion followed by 2 h of reperfusion. The size of the area at risk, identified by the absence of Evans blue staining, was not significantly different between control and CypD-deficient hearts (Fig. 4f). In control hearts, I/R injury caused significant necrotic damage, as evidenced by a large area of myocardium that was negative for triphenyltetrazolium chloride (TTC) staining (Fig. 4e, g). In CypD-deficient hearts, however, the infarct area was dramatically reduced (Fig. 4e, g). Consistently, lactate dehydrogenase (LDH) release due to disruption of the plasma membrane was almost completely inhibited in CypD-deficient hearts (Fig. 4h). These results indicate that lack of CypD can markedly reduce cardiac I/R injury.

An increase in the permeability of the outer mitochondrial membrane is central to apoptotic signalling, and is directly regulated by the Bcl-2 family of proteins[1]. It has been suggested that the mPT plays a role in apoptotic mitochondrial membrane permeabilization[22]. However, we show here that cytochrome *c* release induced by Bid and Bax is not blocked by CypD deficiency and that CypD deficiency does not affect many forms of apoptotic cell death, indicating that the CypD-dependent mPT does not play a significant role in apoptosis in general; however, this does not exclude the possibility that certain forms of apoptosis are mediated by the mPT, and thereby inhibited by CsA. On the other hand, CypD deficiency blocks Ca^{2+}-induced and oxidative stress-induced cytochrome *c* release from isolated mitochondria and also prevents necrotic cell death induced by these stimuli; this indicates that the CypD-dependent mPT is a critical event in some forms of cellular

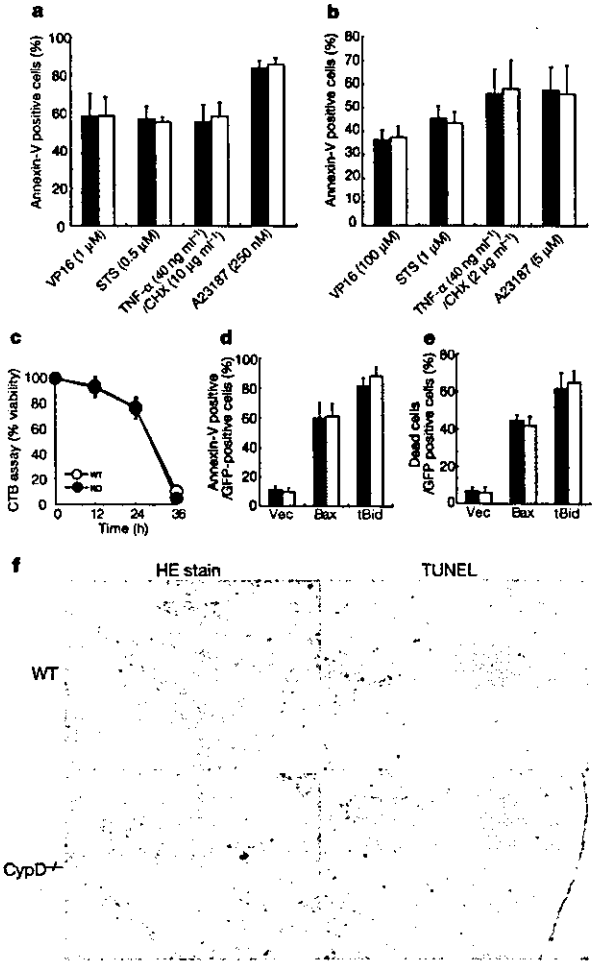

Figure 2 No resistance of Cyp $D^{-/-}$ cells to multiple apoptotic stimuli **a**, **b**, Susceptibility of primary thymocytes and MEFs to various apoptotic stimuli. Wild-type (black) and Cyp $D^{-/-}$ (grey) thymocytes (**a**) and MEFs (**b**) were exposed to apoptosis-inducing reagents for 24 h, and apoptotic cells were assessed by Annexin-V staining. Reagents: etoposide (VP16), staurosporin (STS), tumour-necrosis factor-α (TNF-α) + cycloheximide (CHX), A23187. **c**, Susceptibility of primary hepatocytes to 10 μM STS. Wild-type and $CypD^{-/-}$ hepatocytes were treated with STS for 36 h and cell death was assessed using the CTB assay. Data shown as mean ± s.e.m. **d**, **e**, No effect of CypD deficiency on Bax- or tBid-induced death of MEFs and hepatocytes. Immortalized MEFs (**d**) and primary cultured hepatocytes (**e**) were transiently transfected with DNA for Bax (1 μg) or tBid (1 μg) plus enhanced green fluorescent protein (EGFP, 0.5 μg) for 24 h, and cells were stained with Cy3-conjugated Annexin-V. The percentage of Annexin-V positive cells was calculated relative to all GFP-positive cells. Data shown as mean ± s.e.m. **f**, No effect of CypD deficiency on X-ray-induced apoptosis in the small intestine. Wild-type and $CypD^{-/-}$ mice were exposed to 10 Gy irradiation. After 72 h, a segment of the small intestine was excised and subjected to haematoxylin-eosin (HE) and TUNEL staining.

letters to nature

necrosis. Notably, overexpressed CypD can induce necrosis[23].

We showed that lack of CypD markedly suppresses cardiac I/R injury (which mimics cardiac infarction). In I/R injury, production of reactive oxygen species and Ca^{2+} overload are known to be key events[17]. Our results indicate that CypD-deficient mitochondria can accumulate excess Ca^{2+} without loss of $\Delta\Psi$ and that they also tolerate oxygen radical-induced damage. Consistently, CypD-deficient hepatocytes accumulated more Ca^{2+} than wild-type hepatocytes, and were significantly more resistant to A23187- and H_2O_2-induced death. Thus, the CypD-dependent mPT is a critical event in I/R injury, suggesting that CypD and the mPT may be important therapeutic targets for preventing myocardial infarction. □

Methods

Generation of cyclophilin D-deficient mice

A genomic clone (pKOS 63) containing the CypD locus was isolated from a 129/J mouse genomic library. Lex-1 embryonic stem (ES) cells (derived from the 129SvEvBrd strain)

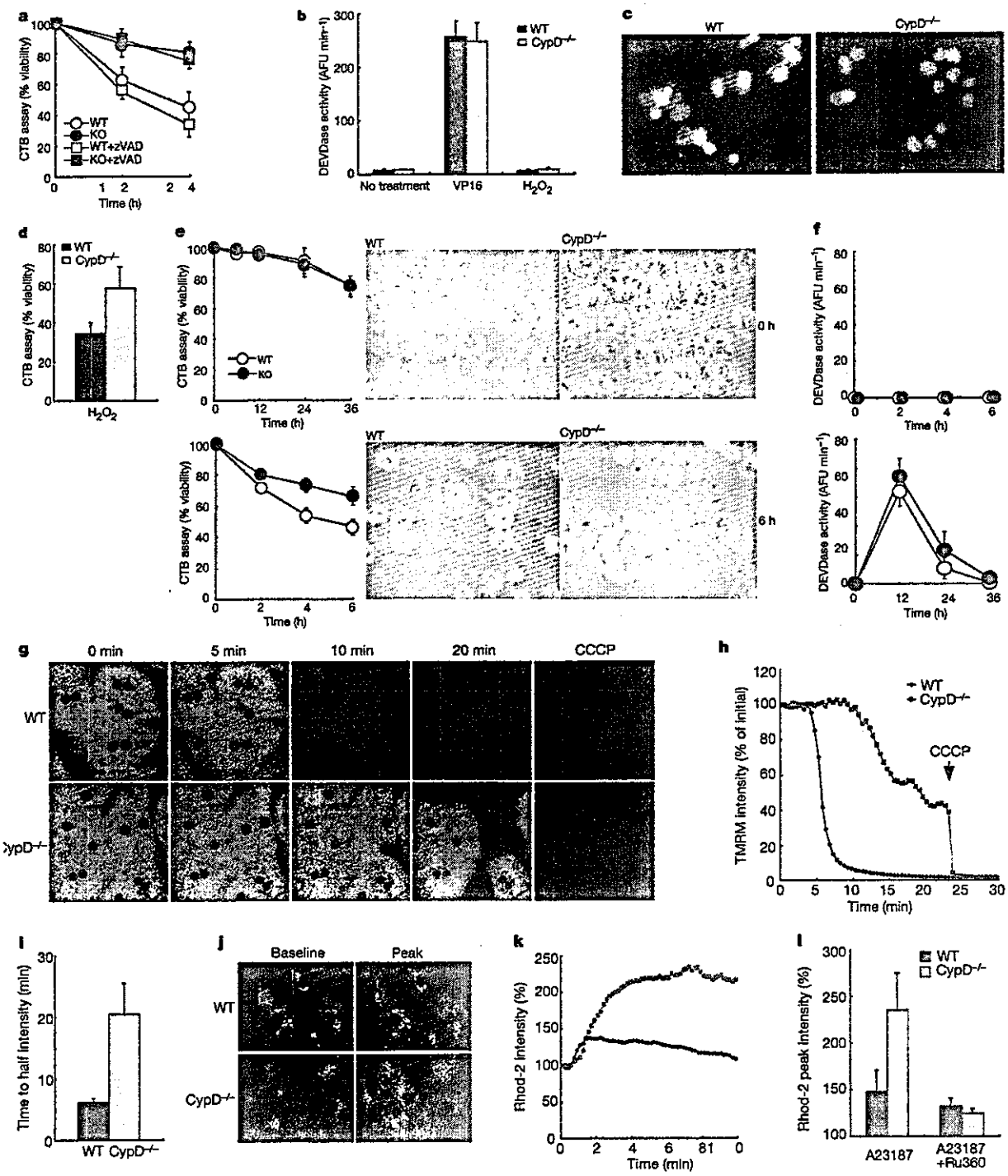

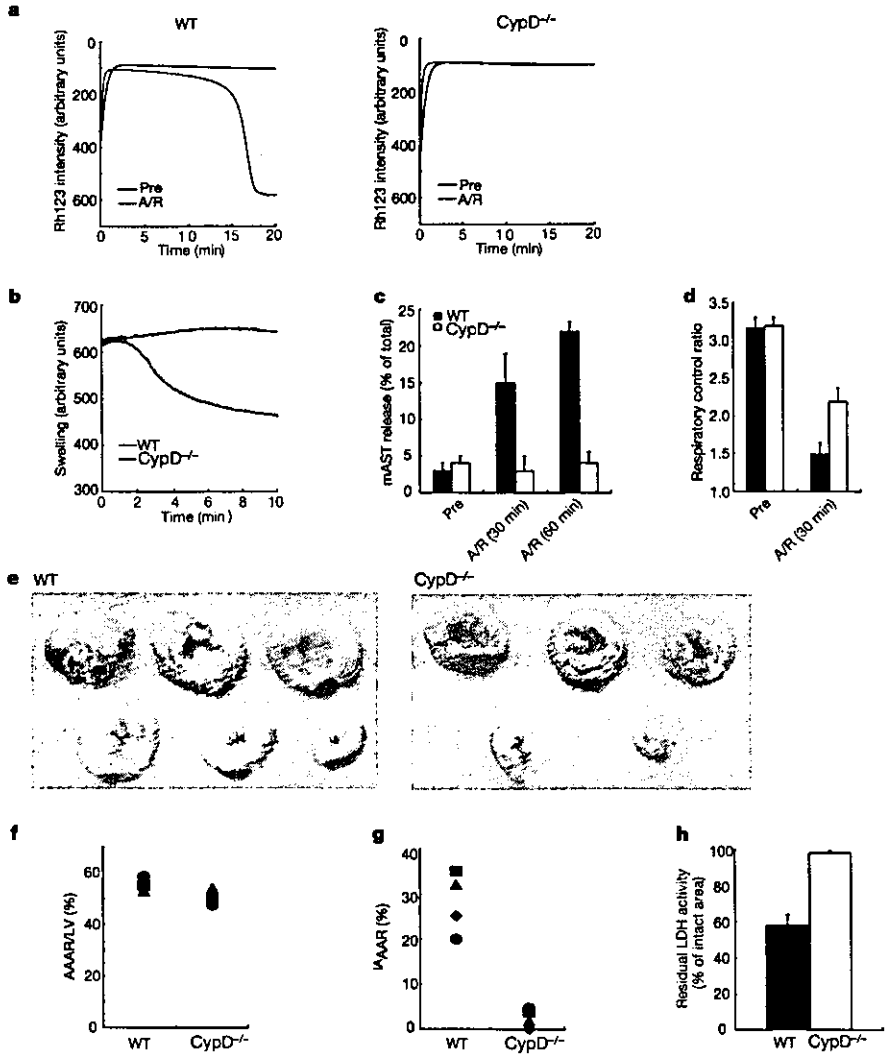

Figure 4 Prevention of cardiac ischaemia/reperfusion injury in CypD$^{-/-}$ mice. **a**–**d**, Absence of mitochondrial damage induced by anoxia/reoxygenation (A/R) in CypD$^{-/-}$ mitochondria. Isolated mitochondria were treated without (Pre) or with anoxia for 30 min followed by reoxygenation for the indicated times. The $\Delta\Psi$ (**a**), swelling (**b**), mAST release (**c**), and respiratory control ratio (state 3/state 4) (**d**) were measured. Data shown as mean ± s.e.m. **e**–**h**, Reduction of cardiac I/R injury in CypD$^{-/-}$ mice. **e**, Representative slices of a heart subjected to I/R. The slices were double-stained with Evans blue (blue) and TTC (red). The infracted region was not stained (white). **f**, The area at risk/left ventricle (AAR/LV) and (**g**) the infarct area/area at risk (IA/AAR). Data are shown for four independent experiments. **h**, The ratio of residual LDH activity in the IA/non-ischaemic area. Data shown as mean ± s.e.m.

Figure 3 Resistance of CypD$^{-/-}$ cells to necrosis induced by reactive oxygen species and Ca^{2+} overload. **a**–**d**, Reduction of H_2O_2-induced necrotic cell death by CypD deficiency. Wild-type (WT) and CypD$^{-/-}$ MEFs (**a**–**c**) and hepatocytes (**d**) were exposed to H_2O_2 (**a**–**c**, 0.75 mM for 24 h; **d**, 0.5 mM for 4 h), and the extent of cell death was assessed by CTB assay (**a**, **d**). zVAD is a pan-caspase inhibitor. **b**, Caspase activation in wild-type (black) and CypD$^{-/-}$ (grey) hepatocytes after treatment with 0.75 mM H_2O_2 was assessed at 16 h. Treatment with VP16 (100 μM) for 16 h was used as a positive control for caspase activation. **c**, Representative nuclear changes visualized by staining with Hoechst 33342 (blue) and PI (red) at 12 h. Data shown as mean ± s.e.m. **e**, WT (filled circles) and CypD$^{-/-}$ (open circles) hepatocytes left untreated (top panel) or treated with 2 μM A23187 (bottom panel), measured using the CTB assay. Data shown as mean ± s.e.m. Phase contrast microscopy images at 0 h and 6 h are shown. **f**, Assessment of caspase activation in response to 2 μM A23187 (left panel); treatment with 40 ng ml^{-1} TNF-α + 10 μg ml^{-1} CHX was used as a positive control for caspase activation (right panel). Data shown as mean ± s.e.m. **g**–**i**, Reduced $\Delta\Psi$ loss in CypD$^{-/-}$ hepatocytes (preloaded with TMRM) treated with 10 μM A23187. TMRM fluorescence intensity was monitored by laser scanning confocal microscopy. Representative real-time images (**g**), average TMRM intensity of individual WT (blue) and CypD$^{-/-}$ (pink) cells (**h**), and the half-life time of the fluorescence intensity of individual cells (**i**) are shown. Data shown as mean ± s.d. The arrow in (**h**) indicates the addition of 5 μM CCCP, which completely dissipated $\Delta\Psi$. **j**–**l**, Increased A23187-induced mitochondrial Ca^{2+} uptake by CypD$^{-/-}$ hepatocytes. Cells were loaded with Rhod2-AM and treated with 10 μM A23187. Rhod2 fluorescence intensity was monitored by laser scanning confocal microscopy. Representative images of baseline and peak fluorescence are shown (**j**). Average (**k**) and peak (**l**) fluorescence intensities of cells are shown (mean ± s.d.). In (**l**), hepatocytes were loaded with Rhod2-AM in the presence of 1 μM Ru360.

were electroporated with the targeting vector and selected by G418. ES clones with the targeted CypD allele were screened by polymerase chain reaction (PCR) and Southern blotting analysis. Heterozygous mutant ES cells were injected into C57BL/6J blastocysts. Germline transmission of mutant alleles to F_1 offspring was confirmed by PCR and Southern blotting, and F_2 offspring from heterozygous intercrosses were genotyped by PCR and Southern blotting.

Genotyping by PCR

The CypD locus was genotyped by PCR. The wild-type allele (553 base pairs, bp) was detected using a forward primer (5′-GCAGATCAAGCTCCCGACTG-3′) and a reverse primer (5′-ACTTGGGAAGCCGAGGTG-3′). To detect the mutant allele (206 bp), a neomycin-specific reverse primer (5′-GCAGCGCATCGCCTTCTATC-3′) was used in combination with the wild-type reverse primer described above.

Antibodies

Anti-mouse CypD antibody was produced using a peptide (amino acids 43–57) of CypD. Anti-cytochrome *c*, anti-cyclophilin A and anti-GAPDH antibodies were purchased from Pharmingen, UpState and Biogenesis, respectively.

Mitochondrial biochemical parameters

Mitochondria were isolated from mouse livers as described previously[21]. In all experiments, except for assessment of respiration, mitochondria were in medium containing 0.3 mM mannitol, 10 mM potassium HEPES (pH 7.4), 0.2 mM EDTA, 0.1% fatty acid-free BSA, 300 μM potassium phosphate (pH 7.4) and 4.2 mM succinate.

Mitochondrial PPIase activity was measured as described previously[21], except that the final concentration of the synthetic peptide substrate (succinyl-Ala-Ala-Pro-Phe-4-nitroanilide) was 75 μM. The activity was expressed as K/K_0, where K and K_0 are the first-order rate constants in the presence and absence of the mitochondrial lysate, respectively. The mitochondrial membrane potential ($\Delta\Psi$) was assessed by measuring the $\Delta\Psi$-dependent uptake of rhodamine 123 (Rh123, ref. 24). Mitochondrial swelling was monitored by the decrease of 90° light scatter at 520 nm, which was determined using a spectrophotometer (Hitachi F-4500). Mitochondrial respiration was measured with an O_2 electrode (Rank Brothers) in respiration buffer[21]. The external mitochondrial Ca^{2+} concentration was monitored using a Ca^{2+}-specific electrode (Orion). The amount of intra-mitochondrial Ca^{2+} was measured using $^{45}Ca^{2+}$. Isolated mitochondria were incubated with $^{45}Ca^{2+}$ for 25 min, and then the mitochondria (1 mg protein) were centrifuged at 12,000*g* for 3 min. The pellet and supernatant fractions were collected and their radioactivity measured using a liquid scintillation counter (Wallac 1409). Cytochrome *c* release was determined as previously described[12].

In anoxia/reoxygenation experiments, mitochondria were suspended in a tube and treated with 100% N_2 gas. The gas-saturated tube was sealed with parafilm and left for 30 min, and the mitochondria were then reoxygenated by shaking in a 12-well plate at room temperature for 30 min.

Cell death assay

Primary cultures of MEFs were obtained from CypD-deficient and control littermate embryos at embryonic day 14.5. MEFs immortalized by SV40 T antigen were also used. Hepatocytes were isolated from CypD-deficient mice and their control littermates at 3–4 months of age using the retrograde two-step collagenase perfusion technique[26]. Cell viability was assessed by propodium iodide (PI) staining, Annexin-V staining or the cell titer blue (CTB) assay. Briefly, cells were stained with 1 μM PI or 1 μM Cy3-conjugated Annexin-V for 5 min at room temperature and were analysed using a flow cytometer (Becton-Dickinson). The CTB assay, which measures the metabolic activity of viable cells, was carried out using Cell Titer Blue reagent (Promega). The nuclear morphology was observed with 10 μM Hoechst 33342 and 1 μM PI staining as described previously[27]. DEVDase activity (cleavage of the caspase-3 substrate DEVD-amc) was measured as described elsewhere[28].

Q4

Laser scanning confocal microscopy

Hepatocytes were cultured in covered glass-bottomed 24-well dishes coated with type I collagen (Iwaki glass) for 16–20 h. To monitor mitochondrial $\Delta\Psi$, hepatocytes were loaded with 0.25 μM TMRM (Molecular Probes) as described previously[29]. To monitor the mitochondrial Ca^{2+} level, hepatocytes were loaded with 5 μM Rhod2-AM (Molecular Probes) in culture medium containing 0.05% Pluronic F-127 (Molecular Probes) and 0.1 mM sulfypizrazone for 2 h at 4 °C for mitochondria-selective loading as described previously[16].

Ischaemia/reperfusion experiments

Using CypD-deficient and wild-type littermate mice at 10–12 weeks of age, ischaemia/reperfusion of the heart was performed as described previously[30]. Briefly, under general anaesthesia with mechanical ventilation, a silk thread (7-0) was passed around the left coronary artery (LCA) about 1 mm distal to the LCA origin to make a snare. After 30 min ligation of the LCA, the snare was released for 2 h. The infarct size was evaluated by double staining using Evans blue dye and triphenyltetrazolium chloride (TTC). The area at risk was defined as the ratio of the area of the ischaemic region to the left ventricular area, and the infarct size was defined as the ratio of the area of the infracted region to that of the ischaemic region.

Statistical evaluation

Statistical evaluation was performed by unpaired *t*-tests. Data are presented as mean ± s.e.m. except for the data shown in Fig. 3i and l, which are shown as mean ± s.d.

Received 2 September 2004; accepted 4 January 2005; doi:10.1038/nature03317.

1. Tsujimoto, Y. Cell death regulation by the Bcl-2 protein family in the mitochondria. *J. Cell. Physiol.* **195**, 158–167 (2003).
2. Green, D. R. & Kroemer, G. The pathophysiology of mitochondrial cell death. *Science* **305**, 626–629 (2004).
3. Halestrap, A. P., McStay, G. P. & Clarke, S. J. The permeability transition pore complex: another view. *Biochimie* **84**, 153–166 (2002).
4. Crompton, M. On the involvement of mitochondrial intermembrane junctional complexes in apoptosis. *Curr. Med. Chem.* **10**, 1473–1484 (2003).
5. Kokoszka, J. E. *et al.* The ADP/ATP translocator is not essential for the mitochondrial permeability transition pore. *Nature* **427**, 461–465 (2004).
6. Halestrap, A. P. Mitochondrial permeability: dual role for the ADP/ATP translocator? *Nature* [online] **430**, 983 (2004) (doi:10.1038/nature02816).
7. Galat, A. & Metcalfe, S. M. Peptidylproline cis/trans isomerases. *Prog. Biophys. Mol. Biol.* **63**, 67–118 (1995).
8. Broekemeier, K. M., Dempsey, M. E. & Pfeiffer, D. R. Cyclosporin A is a potent inhibitor of the inner membrane permeability transition in liver mitochondria. *J. Biol. Chem.* **264**, 7826–7830 (1989).
9. He, L. & Lemasters, J. J. Regulated and unregulated mitochondrial permeability transition pores: a new paradigm of pore structure and function? *FEBS Lett.* **512**, 1–7 (2002).
10. Scorrano, L. *et al.* A distinct pathway remodels mitochondrial cristae and mobilizes cytochrome c during apoptosis. *Dev. Cell* **2**, 55–67 (2002).
11. Wei, M. C. *et al.* Proapoptotic BAX and BAK: a requisite gateway to mitochondrial dysfunction and death. *Science* **292**, 727–730 (2001).
12. Narita, M. *et al.* Bax interacts with the permeability transition pore to induce permeability transition and cytochrome c release in isolated mitochondria. *Proc. Natl Acad. Sci. USA* **95**, 14681–14686 (1998).
13. Eskes, R. *et al.* Bax-induced cytochrome C release from mitochondria is independent of the permeability transition pore but highly dependent on Mg^{2+} ions. *J. Cell Biol.* **143**, 217–224 (1998).
14. Finucane, D. M., Bossy-Wetzel, E., Waterhouse, N. J., Cotter, T. G. & Green, D. R. Bax-induced caspase activation and apoptosis via cytochrome c release from mitochondria is inhibitable by Bcl-xL. *J. Biol. Chem.* **274**, 2225–2233 (1999).
15. von Ahsen, O. *et al.* Preservation of mitochondrial structure and function after Bid- or Bax-mediated cytochrome c release. *J. Cell Biol.* **150**, 1027–1036 (2000).
16. Trollinger, D. R., Cascio, W. E. & Lemasters, J. J. Selective loading of Rhod 2 into mitochondria shows mitochondrial Ca^{2+} transients during the contractile cycle in adult rabbit cardiac myocytes. *Biochem. Biophys. Res. Commun.* **236**, 738–742 (1997).
17. Weiss, J. N., Korge, P., Honda, H. M. & Ping, P. Role of the mitochondrial permeability transition in myocardial disease. *Circ. Res.* **93**, 292–301 (2003).
18. Shimizu, S. *et al.* Beneficial effects of cyclosporine on reoxygenation injury in hypoxic rat liver. *Transplantation* **57**, 1562–1566 (1994).
19. Javadov, S. A. *et al.* Ischaemic preconditioning inhibits opening of mitochondrial permeability transition pores in the reperfused rat heart. *J. Physiol. (Lond.)* **549**, 513–524 (2003).
20. Matsumoto, S., Friberg, H., Ferrand-Drake, M. & Wieloch, T. Blockade of the mitochondrial permeability transition pore diminishes infarct size in the rat after transient middle cerebral artery occlusion. *J. Cereb. Blood Flow Metab.* **19**, 736–741 (1999).
21. Khaspekov, L., Friberg, H., Halestrap, A., Viktorov, I. & Wieloch, T. Cyclosporin A and its nonimmunosuppressive analogue N-Me-Val-4-cyclosporin A mitigate glucose/oxygen deprivation-induced damage to rat cultured hippocampal neurons. *Eur. J. Neurosci.* **11**, 3194–3198 (1999).
22. Zamzami, N. & Kroemer, G. The mitochondrion in apoptosis: how Pandora's box opens. *Nature Rev. Mol. Cell Biol.* **2**, 67–71 (2001).
23. Li, Y., Johnson, N., Capano, M., Edwards, M. & Crompton, M. Cyclophilin-D promotes the mitochondrial permeability transition but has opposite effects on apoptosis and necrosis. *Biochem. J.* **383**, 101–109 (2004).
24. Shimizu, S. *et al.* Bcl-2 prevents apoptotic mitochondrial dysfunction by regulating proton flux. *Proc. Natl Acad. Sci. USA* **95**, 1455–1459 (1998).
25. Fischer, G., Wittmann-Liebold, B., Lang, K., Kiefhaber, T. & Schmid, F. X. Cyclophilin and peptidyl-prolyl *cis-trans* isomerase are probably identical proteins. *Nature* **337**, 476–478 (1989).
26. Hatano, E. *et al.* The mitochondrial permeability transition augments Fas-induced apoptosis in mouse hepatocytes. *J. Biol. Chem.* **275**, 11814–11823 (2000).
27. Shinzawa, K. & Tsujimoto, Y. PLA2 activity is required for nuclear shrinkage in caspase-independent cell death. *J. Cell Biol.* **163**, 1219–1230 (2003).
28. Shimizu, S., Eguchi, Y., Kamiike, W., Matsuda, H. & Tsujimoto, Y. Bcl-2 expression prevents activation of the ICE protease cascade. *Oncogene* **12**, 2251–2257 (1996).
29. Byrne, A. M., Lemasters, J. J. & Nieminen, A. L. Contribution of increased mitochondrial free Ca^{2+} to the mitochondrial permeability transition induced by tert-butylhydroperoxide in rat hepatocytes. *Hepatology* **29**, 1523–1531 (1999).
30. Yamashita, N. *et al.* Exercise provides direct biphasic cardioprotection via manganese superoxide dismutase activation. *J. Exp. Med.* **189**, 1699–1706 (1999).

Supplementary Information accompanies the paper on **www.nature.com/nature.**

Acknowledgements We are grateful to K. Tagawa for helpful discussion and C. Thompson for providing Bak-deficient mice. CypD-deficient mice were developed in collaboration with Lexicon Genetics Incorporated. This study was supported in part by a grant for Scientific Research on Priority Areas, a grant for Center of Excellence Research, a grant for the 21st century COE Program, a grant for Scientific Research from the Ministry of Education, Science, Sports, and Culture of Japan, and by a grant for Research on Dementia and Fracture from the Ministry of Health, Labour and Welfare of Japan.

Competing interests statement The authors declare that they have no competing financial interests.

Correspondence and requests for materials should be addressed to Y.T. (tsujimot@gene.med.osaka-u.ac.jp)

Journal of Neurochemistry, 2004, **90**, 1402–1413 doi:10.1111/j.1471-4159.2004.02597.x

PEN-2 enhances γ-cleavage after presenilin heterodimer formation

Hirohisa Shiraishi,*,† Xiaorei Sai,*,[1] Hua-Qin Wang,‡ Yasuhiro Maeda,§ Yukihisa Kurono,§ Masaki Nishimura,‡ Katsuhiko Yanagisawa* and Hiroto Komano*

*Department of Dementia Research, National Institute for Longevity Sciences, Morioka, Obu, Aichi, Japan
†Organization for Pharmaceutical Safety and Research of Japan, Chiyoda-ku, Tokyo, Japan
‡Molecular Neuroscience Research Center, Shiga University of Medical Science, Otsu, Shiga, Japan
§Faculty of Pharmaceutical Sciences, Nagoya City University, Nagoya, Aichi, Japan

Abstract

The presenilin (PS) complex, including PS, nicastrin, APH-1 and PEN-2, is essential for γ-secretase activity, which is required for amyloid β-protein (Aβ) generation. However, the precise individual roles of the three cofactors in the PS complex in Aβ generation remain to be clarified. Here, to distinguish the roles of PS cofactors in γ-secretase activity from those in PS endoproteolysis, we investigated their roles in the γ-secretase activity reconstituted by the coexpression of PS N- and C-terminal fragments (NTF and CTF) in PS-null cells. We demonstrate that the coexpression of PS1 NTF and CTF forms the heterodimer and restores Aβ generation in PS-null cells. The generation of Aβ was saturable at a certain expression level of PS1 NTF/CTF, while the overexpression of PEN-2 alone resulted in a further increase in Aβ generation. Although PEN-2 did not enhance PS1 NTF/CTF heterodimer formation, PEN-2 expression reduced the IC_{50} of a specific γ-secretase inhibitor, a transition state analogue, for Aβ generation, suggesting that PEN-2 expression enhances the affinity or the accessibility of the substrate to the catalytic site. Thus, our results strongly suggest that PEN-2 is not only an essential component of the γ-secretase complex but also an enhancer of γ-cleavage after PS heterodimer formation.

Keywords: Alzheimer's disease, amyloid β-protein, nicastrin, PEN-2, APH-1, presenilin.
J. Neurochem. (2004) **90**, 1402–1413.

In the brains of patients with Alzheimer's disease, the fundamental neuropathological change is the abnormal deposition of amyloid β-protein (Aβ) (for review, see Selkoe 1999). Aβ is generated from β-amyloid precursor protein (APP) through its sequential proteolytic cleavage catalysed by β- and γ-secretases (for review, see Selkoe 1999). β-secretase was identified as a membrane-tethered aspartyl protease (Vassar *et al.* 1999), whereas the molecules responsible for γ-secretase activity were found to be the presenilin (PS) complex, including PS, nicastrin (NCT) (Yu *et al.* 2000b), APH-1 (Goutte *et al.* 2002) and PEN-2 (Francis *et al.* 2002).

Mutations in the PS genes, *PS1* and *PS2*, cause early onset familial Alzheimer's disease (reviewed in Selkoe 1999). PS is required not only for γ-secretase activity (De Strooper *et al.* 1998; Herreman *et al.* 2000; Zhang *et al.* 2000) but also several intramembranous cleavages, including those of APP named as ε-cleavage (Gu *et al.* 2001; Sastre *et al.* 2001; Weidemann *et al.* 2002), Notch (De Strooper *et al.* 1999; Zhang *et al.* 2000), ErbB-4 (Lee *et al.* 2001; Ni *et al.* 2001), Cadherin (Marambaud *et al.* 2002, 2003), and CD44 (Lammich *et al.* 2002; Murakami *et al.* 2003). These results suggest that PS-mediated intramembranous cleavage plays a critical role in biological functions. PS has been proposed to have the catalytic site of γ-secretase; it contains two conserved, essential aspartate residues in adjacent transmembrane domains that may define a novel aspartyl protease active site (Wolfe *et al.* 1999; Li *et al.* 2000b; Steiner *et al.* 2000; Weihofen *et al.* 2002). PS is processed to an active,

Received February 18, 2004; revised manuscript received April 27, 2004; accepted May 11, 2004.

Address correspondence and reprint requests to Hiroto Komano, Department of Dementia Research, National Institute for Longevity Sciences, 36-3 Gengo, Morioka, Obu, Aichi 474-8522, Japan.
E-mail: hkomano@nils.go.jp
[1]The present address of Xiaorei Sai is Laboratory for Sensory Development, RIKEN-Center for Developmental Biology, Chuo-ku, Kobe 656-0047, Japan.

Abbreviations used: Aβ, amyloid β-protein; APP, β-amyloid precursor protein; CTF, C-terminal fragment; DAPT, *N*-[*N*-(3,5-difluorophenylacetyl)-L-alanyl]-*S*-phenylglycine *t*-butyl ester; ELISA, enzyme-linked immunosorbent assay; IC50, 50% inhibitory concentration; NCT, nicastrin; NTF, N-terminal fragment; PS, presenilin; RIPA, radioimmunoprecipitation assay.

stable form by endoproteolysis and the cellular level of processed PS is tightly limited (Ratovitski *et al.* 1997; Thinakaran *et al.* 1997). The processed PS resides in a high molecular weight complex that includes mature glycocylated NCT, APH-1 and PEN-2 (Yu *et al.* 2000b; Edbauer *et al.* 2002; Esler *et al.* 2002; Yang *et al.* 2002; Kimberly *et al.* 2003; Takasugi *et al.* 2003).

Several lines of evidence have clearly established that NCT, APH-1 and PEN-2 (collectively named PS cofactors in this study) are required for PS processing and the formation of the active γ-secretase complex (Francis *et al.* 2002; Lee *et al.* 2002; Steiner *et al.* 2002; Edbauer *et al.* 2003; Hu and Fortini 2003; Kim *et al.* 2003; Kimberly *et al.* 2003; Luo *et al.* 2003; Takasugi *et al.* 2003). In addition, reconstitution experiments in yeast demonstrated that the coexpression of all four components is necessary and sufficient for the reconstitution of γ-secretase activity (Edbauer *et al.* 2003). However, the precise roles of PS cofactors in Aβ generation remain to be elucidated because it is not yet conclusive whether the cofactors are only necessary for PS endoproteolysis and the formation of the active γ-secretase or whether they also play a role in Aβ generation after the formation of the γ-secretase complex. Here, we demonstrate that the coexpression of PS1 N- and C-terminal fragments (NTF and CTF) in PS-null cells (PS1/PS2 double-deficient cells) restores Aβ generation similarly to the expression of PS holoprotein. As the coexpression of PS1 NTF and CTF in PS-null cells allows us to distinguish the roles of PS cofactors in γ-secretase activity from those in PS endoproteolysis, we investigated their roles in the γ-secretase activity reconstituted by the coexpression of PS NTF and CTF in PS-null cells. We noted that PEN-2 expression results in an increase in the extent of Aβ generation restored by the coexpression of PS NTF and CTF in PS-null cells. Thus, we concluded that PEN-2 enhances PS-mediated γ-cleavage after PS NTF/CTF heterodimer formation.

Experimental procedures

Antibodies, reagents and cell lines

The monoclonal antibody 6E10 specific to human Aβ1–17 was purchased from Signet Laboratories, Inc. (Redham, MA, USA). The other Aβ antibodies have all been characterized previously (Asami-Odaka *et al.* 1995). The affinity-purified rabbit antibody, B12/4, was raised against 20 C-terminal amino acid residues of APP695 (De Strooper *et al.* 1995). The anti-APP N-terminal antibody was purchased from Sigma (St Louis, MO, USA). The rat anti-PS1 antibody (for NTF of PS1) and the mouse anti-PS1 loop monoclonal antibody were purchased from Chemicon (Temecula, CA, USA). An anti-NCT antibody was purchased from Affinity BioReagents Inc. (Golde, CO, USA) and Sigma. An anti-myc antibody was purchased from MBL (Nagoya, Japan). Affinity-purified rabbit antibody 369 was raised against the C-terminal residues of APP695 (Buxbaum *et al.* 1990). The rabbit anti-PEN-2 antibody was purchased from Zymed Laboratories Inc. (South San Francisco, CA, USA). PS1/PS2 double-deficient murine fibroblasts (PS-null cells) and wild-type murine fibroblasts immortalized with a large T antigen were maintained as previously described (Herreman *et al.* 2000; Sai *et al.* 2002). A γ-secretase inhibitor, L-685,458, was purchased from Calbiochem (San Diego, CA, USA), *N*-[*N*-(3,5-difluorophenylacetyl)-L-alanyl]-*S*-phenylglycine *t*-butyl ester (DAPT) was purchased from Peptide Institute Inc. (Osaka, Japan) and Compound-E and WPE-III-31C were purchased from Calbiochem (San Diego, CA, USA).

Plasmids and retrovirus-mediated gene expression

N-terminal FLAG-tagged PEN-2 and C-terminal myc-tagged APH-1b (Francis *et al.* 2002) were amplified from the Hela cell cDNA library (Clontech, Palo Alto, CA, USA) by the PCR method. The primer sequences used for the PCR were as follows: primers for N-terminal FLAG-tagged PEN-2, 5′-TTCTGAATTCAACCTGGAGCGAGTGTCCAATGAG-3′ and 5′-TTTTCTCGAGCCCCAGTATGTGCAGAAGTTGTCA-3′; primers for C-terminal myc-tagged APH-1b, 5′-TTTTAAGCTTGTTTCCGCGGTGGCCATGACT-3′ and 5′-TTTTGAGCTCTCTGGAGCGCTGGTTGTAAAG-3′. PEN-2 was amplified by the PCR method using the primers 5′-CGCGGATCCACCATGAACCTGGAGCGAGTGTCCAAT-3′ and 5′-CGCGGATCCATGAACCTGGAGCGAGTGTCCAATGAGGAGAAATTGA-3′. pMX-F-PEN-2 is a *Bam*HI-*Sal*I fragment carrying the sequence encoding the N-terminal FLAG-tagged PEN-2 and Kozac consensus sequence (CCACC) at the 5′ end inserted into the *Bam*HI and *Sal*I sites of a retrovirus vector, pMX (Onishi *et al.* 1996). pMX-PEN-2 is inserted into the *Bam*HI and *Xho*I sites of a pMX. pMX-APH-1b-myc is a 1.4-kb *Bam*HI-*Sal*I fragment carrying the C-terminal myc-tagged APH-1b inserted into the *Bam*HI and *Sal*I sites of pMX. pMX-NCT is a *Bam*HI-*Not*I fragment carrying NCT inserted into the *Bam*HI and *Sal*I sites of pMX. pMX-PS1 is a *Not*I fragment carrying PS1 inserted into the *Not*I site of pMX. pMX-APP695 was generated as previously described (Komano *et al.* 2002). pMX-PS1D385 A is an *Eco*RI-*Xho*I fragment carrying mutant PS1 D385A (Yu *et al.* 2000a) inserted into the *Eco*RI and *Sal*I sites of pMX. The PS1 NTF was amplified using the primers PS1-NR, 5′-CATGCTCGAGCTATGTTGAGGAGTAAATG-3′ and PS1-NF, 5′-TGCAGAATTCATGACAGAGTTACCTGCA-3′. The PS1 CTF was amplified using the primers PS1-CR, 5′-CATGCTCGAGCTAGATATAAAATTGATGG-3′ and PS1-CF, 5′-TGCAGAATTCATGGTGTGGTTGGTGAATA-3′. The PCR products were digested with *Eco*RI and *Xho*I inserted into pMX. The PS NTF containing D257A and PS1 CTF containing D385A were PCR amplified using the primers described above from pMX-D257A and pMX-PS1D385A, respectively. All resulting constructs were verified by DNA sequencing. Retrovirus-mediated gene expression in cells was carried out as previously reported (Onishi *et al.* 1996; Komano *et al.* 2002). The infection efficiency was nearly 100% in this study, as estimated in a control experiment using pMX-GFP (retroviral vector carrying GFP).

Amyloid β-protein detection and other immunoblotting techniques

The secreted Aβ was determined by ELISA as previously described (Asami-Odaka *et al.* 1995). The capture antibody used was BNT77. The detector antibodies used were horseradish peroxidase-conjugated BA27 (for Aβ40) and horseradish peroxidase-conjugated

BC05 (for Aβ42). ELISA data were statistically analysed by ANOVA using StatView-J.4.11 (Abacus Concepts, Inc., Berkeley, CA, USA). Cultured cells were lysed in ristocetin-induced platelet agglutination (RIPA) buffer (150 mM NaCl, 10 mM Tris/HCl, pH 7.5, 1% Nonidet P-40, 0.1% sodium dodecyl sulphate and 0.2% sodium deoxycholate, a protease inhibitor cocktail) or 1% CHAPSO buffer (1% CHAPSO, 150 mM NaCl, 10 mM Tris/HCl, pH 7.5, 2 mM EDTA, a protease inhibitor cocktail). The RIPA-solubilized proteins were subjected to immunoblotting as previously described (Sudoh *et al.* 1998). The CHAPSO-solubilized proteins were subjected to immunoprecipitation as previously described (Sudoh *et al.* 1998; Li *et al.* 2000a).

Results

PEN-2 expression increases amyloid β-protein generation

We first established the effect of exogenous PEN-2 and/or APH-1b expression (Francis *et al.* 2002) on Aβ generation and PS1 endoproteolysis using fibroblasts retrovirally expressing human PS1, NCT and APP. As previously reported, the coexpression of PEN-2, APH-1b and NCT resulted in significant accumulations of PS1 NTF and CTF, accompanied by the stimulation of NCT maturation (Fig. 1a, lane 4), while no effect of PEN-2 or APH-1b expression alone on the steady-state levels of PS1 NTF and CTF was observed (Fig. 1a) (Kim *et al.* 2003; Kimberly *et al.* 2003; Luo *et al.* 2003; Takasugi *et al.* 2003). It appears that the interaction of NCT, APH-1 and PEN-2 with PS permits autoproteolysis and the stimulation of the intracellular trafficking of the complex leading to NCT maturation. However, unexpectedly, the expression of PEN-2 alone significantly increased both the Aβ40 and Aβ42 levels (two- to threefold) (Figs 1a and b). The degree of this increase was equivalent to (or even higher than) that induced by the coexpression of the three components NCT, APH-1 and PEN-2 (Figs 1a and b). Thus, we decided to characterize the increase in Aβ generation caused by exogenous PEN-2 using fibroblasts expressing APP695 (PS, NCT and APH-1, endogenous levels). As shown in Fig. 1(c), even when NCT, APH-1 and PS were at endogenous levels, exogenous PEN-2 expression increased Aβ generation. PEN-2 expression does not increase the level of α- or β-secretase-cleaved soluble APP (Selkoe 1999), indicating that PEN-2 did not enhance α- and β-secretase cleavage. However, the intracellular levels of the β-secretase-cleaved APP CTF (C99) and the α-secretase-cleaved APP CTF (C83), which are the substrates of γ-secretase (Wolfe *et al.* 1999), were decreased by PEN-2 expression (Fig. 1c). We also confirmed that an increase in Aβ generation by PEN-2 expression is completely dependent on PS, as no Aβ was detected in PS-null cells overexpressing PEN-2 (data not shown). We also obtained results showing that HEK293 or N2a cells retrovirally expressing PEN-2 increased Aβ generation [an increase in Aβ generation by the retroviral expression of PEN-2 relative to mock expression (fold): N2a, 1.8 (Aβ40) and 1.7 (Aβ42), $n = 4$, $p < 0.02$; HEK293 expressing APP 695, 1.6 (Aβ40) and 1.6 (Aβ42), $n = 4$, $p < 0.02$]. This result strongly suggested that an increase in Aβ generation by PEN-2 expression occurs in other cell types.

We next determined the effects of various expression levels of PEN-2, APH-1b or NCT on Aβ generation (Fig. 2a) because the capability of the cofactors to increase Aβ generation may be dependent on their expression levels. For this purpose, using various concentrations of the virus solution containing the cofactor cDNA, we investigated the change in the extent of Aβ generation with the expression level of PEN-2, APH-1 or NCT by the retrovirus-mediated expression method. We found that PEN-2 expression increased Aβ generation in a dose-dependent manner while APH-1b inhibited Aβ generation and NCT expression did not affect Aβ generation. We also excluded the possibility that the presence of the FLAG tag on PEN-2 has an effect of enhancing Aβ generation, because PEN-2 without the FLAG tag also increased Aβ generation, as shown in Fig. 2(b). Therefore, we concluded that the expression of PEN-2 can enhance PS-mediated γ-secretase cleavage but this effect appears not to be associated with the stimulation of PS endoproteolysis as suggested in Fig. 1(a).

Thus, we decided to separate the roles of the PS cofactors in γ-secretase activity from those in PS endoproteolysis.

Coexpression of presenilin 1 N- and C-terminal fragments restores amyloid β-protein generation in presenilin-null cells

Previously, it was shown that the coexpression of PS1 NTF and CTF rescues the *sel-12* egg-laying defect, suggesting that the coexpression of PS1 and CTF forms biologically active PS in cells (Levitan *et al.* 2001). However, it was not clarified whether the coexpression of PS1 NTF and CTF forms active γ-secretase in PS-null cells. Therefore, to distinguish the roles of PS cofactors in the PS endoproteolysis and γ-secretase activity, we first determined whether the coexpression of PS1 NTF and CTF in PS-null cells can restore Aβ generation. As shown in Fig. 3(a), the coexpression of PS1 NTF and CTF induced Aβ generation similarly to the expression of PS1 holoprotein, while the expression of PS1 NTF or CTF alone did not restore Aβ generation. This result clearly indicates that the coexpression of PS1 NTF and CTF leads to the formation of a functional complex for γ-secretase activity. The coexpression of PS1 NTF mutated at Asp257 and CTF or PS NTF and CTF mutated at Asp385 did not induce Aβ generation in PS-null cells (Fig. 3b), clearly indicating that either of the aspartate residues located in putative transmembrane domains 6 (TM6) and 7 (TM7) is necessary for γ-secretase activity mediated by the coexpression of PS1 NTF and CTF. We also investigated whether the γ-secretase activity is dependent on the expression levels of

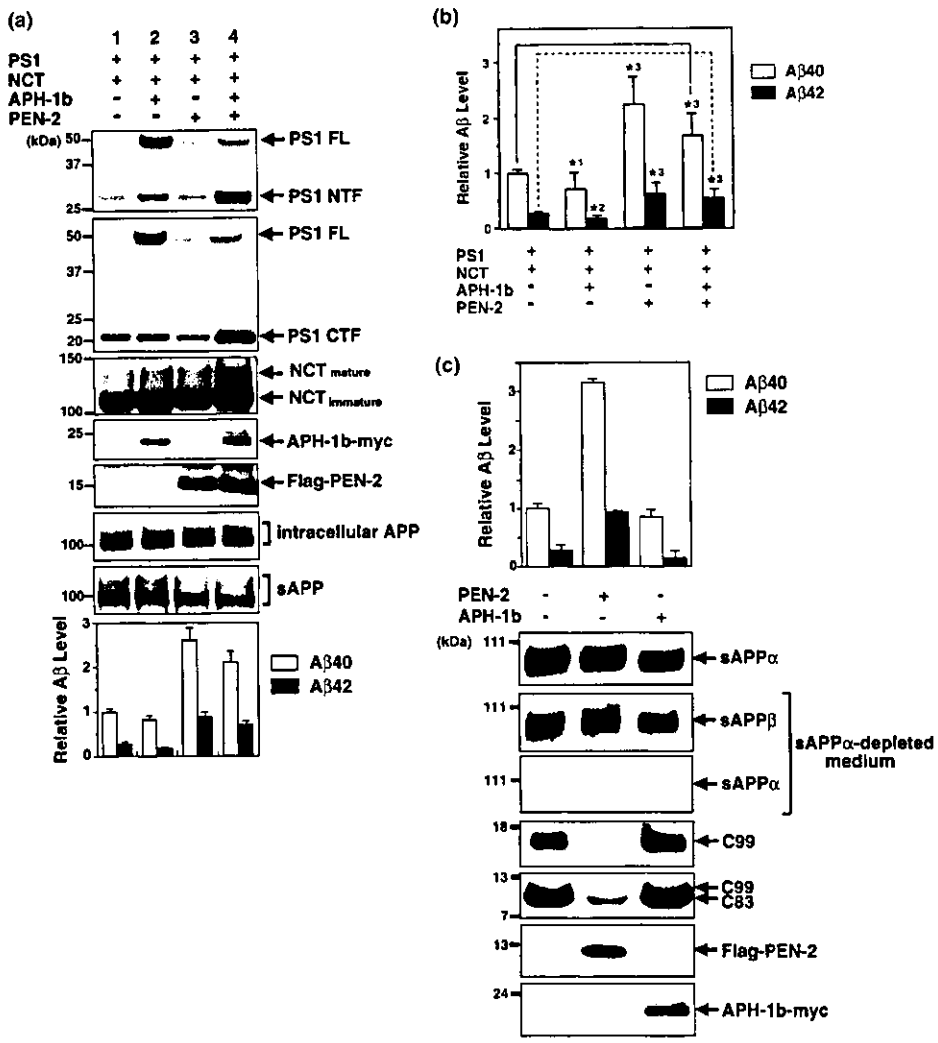

Fig. 1 Exogenous PEN-2 enhances amyloid β-protein (Aβ) generation. (a) Effect of exogenous PEN-2 and/or APH-1b on presenilin (PS)1 endoproteolysis and Aβ generation. Murine fibroblasts (2×10^5) retrovirally expressing β-amyloid precursor protein (APP)695 were plated on a 100-mm tissue culture dish. After the indicated exogenous genes were retrovirally expressed, the RIPA-solubilized lysates (25 μg) were immunoblotted with the anti-PS1 N-terminal fragment (NTF) antibody, anti-PS1 loop antibody, anti-nicastrin (NCT) antibody, anti-FLAG antibody (for FLAG-tagged PEN-2), anti-myc antibody (for myc-tagged APH-1b) and anti-APP antibody, 6E10. Soluble APP (sAPP) was immunoblotted with anti-APP antibody 22C11. Aβ40 and Aβ42 secreted from the cells during a 48-h culture were quantified by ELISA. Values are means ± SD of two independent dishes ($n = 2$). The intensities of the band corresponding to sAPP were quantified densitometrically using NIH Image software (National Institute of Health, Bethesda, MA, USA). The Aβ level was normalized to sAPP in each experiment. The normalized levels were expressed as relative to basal Aβ40 levels obtained from the cells expressing NCT and PS1. +, retrovirus-mediated expression of the indicated exogenous cDNAs; −, mock infection (retroviral vector, pMX, alone). PEN-2, N-terminally FLAG-tagged PEN-2 (FLAG-PEN-2); APH-1b, C-terminally myc-tagged APH-1b (APH-1b-myc); PS1 FL, PS1 full-length; PS1 NTF, PS1 N-terminal fragment; PS1 CTF, PS1 C-terminal fragment. The CTF level of endogenous PS1 in mock-transfected cells (pMX alone) was similar to that of exogenous PS1 observed in lane 1, probably caused by the replacement of the endogenous PS1 with exogenous PS1 as previously shown (Thinakaran *et al.* 1996, 1997) (data not shown). (b) The statistical analysis of Aβ levels of the six independent experiments ($n = 6$). Significant difference at $^{*1}p < 0.05$, $^{*2}p < 0.01$ and $^{*3}p < 0.005$ (Mann–Whitney *U*-test). (c) Exogenous PEN-2 expression alone enhances γ-cleavage. After PEN-2 or APH-1b was retrovirally expressed in fibroblasts (2×10^5) expressing APP695 (PS and NCT, endogenous levels), Aβ40 and Aβ42 secreted from cells during a 48-h culture were quantified by ELISA. The Aβ level was normalized to sAPP in each experiment. The normalized levels were expressed as relative to basal Aβ40 levels obtained from the mock-transfected cells as described in (a). The medium used for the 48-h culture was immunoblotted with 6E10 (for sAPPα). The sAPPα-depleted medium was immunoblotted with the anti-APP-N-terminal antibody (for sAPPβ) and with 6E10 (for the confirmation of sAPPα depletion). Intracellular C99 in RIPA-solubilized lysates (1.5 mg) was immunoprecipitated with BAN50 and immunodetected with B12/4 as previously described (Sai *et al.* 2002). Intracellular C83 in RIPA-solubilized lysates (1.5 mg) was immunodetected with the antibody against the APP C-terminal fragment 369. Data are representative of three independent experiments.